Journal of Mathematical Modeling
Vol. -, No. -, 2026, pp. -. Research Article

JMM

Numerical analysis of American put option pricing using free boundary methods: Applications to Indian banking sector data

S. Asati[†], R.K. Gangele[†], K.C. Patidar[§*]

[†]*Department of Mathematics, Dr. Harisingh Gour Vishwavidyalaya, Sagar, India*
[§]*Department of Mathematics and Applied Mathematics, University of the Western Cape, South Africa*

Email(s): shivangiasati25@gmail.com, rkgangele23@gmail.com, kpatidar@uwc.ac.za

Abstract. We develop a computational framework for pricing American put options that combines a front-tracking technique with the Black-Scholes PDE to determine the optimal exercise boundary. The logarithmic variable $x = \ln(S/S_f(\tau))$ transforms the problem to a fixed domain in which the velocity term $S_f'(\tau)/S_f(\tau)$ and an exact update equation for the free boundary appear explicitly; the grid moves with the exercise boundary, the velocity term is integrated along characteristics, and explicit, fully implicit and Crank-Nicolson schemes are employed. The analysis is restricted to the linear steps of the method for a prescribed boundary position. For the linear diffusion update we prove local consistency, von Neumann and ℓ_2-stability and a discrete maximum principle by an exact (not frozen-coefficient) analysis; for the interpolation along characteristics we prove a one-step error estimate whose constant does not depend on the shift or the mesh size, and the von Neumann stability of a single transfer step. No stability or convergence theorem is proved for the fully coupled nonlinear free-boundary algorithm; its behaviour is assessed only numerically. The errors are measured against independent references: an integral-equation solution for option values and the exercise boundary, the binomial model with Richardson extrapolation and Longstaff-Schwartz least-squares Monte Carlo. The framework is applied, in a model-parameter study of hypothetical American puts, to three- and six-month unadjusted daily closing prices of four major Indian banks, using close-to-close volatilities and the Reserve Bank of India policy rate as risk-free rate. Sensitivity to these inputs, a dividend yield, the boundary-update procedure and moneyness is quantified.

Keywords: American options; free boundary problems; front-tracking methods; finite difference schemes; stability of linear steps; Indian financial market
AMS Subject Classification 2010: 39A05, 65M06, 65M12, 91G60.

*Corresponding author
Received: 15 August 2026/ Revised: 22 November 2026/ Accepted: 23 November 2026
DOI: 10.22124/jmm.2026.34172.3149

© 2026 University of Guilan

Corrected Proof

1 Introduction

Option pricing problems have attracted considerable attention over the past four decades, resulting in the development of numerous mathematical models and computational methodologies. These approaches are generally designed for specific classes of problems and possess their own advantages and limitations. For complex financial models involving multidimensional stochastic processes, Monte Carlo simulation-based techniques are often preferred due to their flexibility and ability to handle high-dimensional problems. Although computationally expensive, these methods remain valuable when deterministic approaches become impractical. However, for low-dimensional problems, such as the single-asset option pricing model considered in this work, finite difference methods provide an efficient and accurate alternative. These methods solve the underlying partial differential equations directly and typically require fewer computational resources than Monte Carlo approaches, which often rely on a large number of simulated paths to achieve comparable accuracy. The present work focuses on pricing American put options in the Indian financial market using a finite difference-based computational framework. These methods remain widely adopted due to their simplicity, robustness, and ability to incorporate early exercise features through free boundary formulations or suitable exercise-continuation criteria. The advantages of finite difference methods extend beyond computational efficiency. As grid-based approaches, they allow direct control of numerical accuracy through grid refinement and provide a natural framework for stability and convergence analysis.

Two families of finite difference methods can be distinguished for the American put. In the first, the problem is posed on a fixed grid as a linear complementarity problem (LCP); the discrete LCP is then solved exactly, e.g., by the Brennan-Schwartz algorithm [2,16], by projected iterations, or approximately by penalty [11] or operator-splitting [14, 15] methods, and the exercise boundary is only recovered a posteriori. In the second, the free boundary S_f is kept as an unknown: a Landau-type change of variables maps the continuation region onto a fixed domain, the boundary velocity S_f'/S_f enters the transformed equation, and the boundary is computed together with the option value at every time level [5, 10, 21, 28]; a fixed-domain transformation is also the starting point of the integral-equation analysis of the free boundary in [27]. The present paper belongs to the second family. Because the computational grid $S_j(\tau) = S_f(\tau)e^{x_j}$ moves with the exercise boundary, we refer to the complete method as a front-tracking method ; the term front fixing is reserved for the change of variables itself (Remark 1). The transformed problem, the treatment of the velocity term and the boundary-update equation are derived in full (see Sections 2 and 3), the fixed-grid LCP formulation is used for comparison, and the stability analysis of the linear steps, for a prescribed boundary position, is carried out for the actual (constant-coefficient) difference operators rather than under a frozen-coefficient assumption (see Section 4).

Relation to the closest front-fixing schemes. The individual components of the present method (a logarithmic Landau transformation, interpolation along characteristics, a ghost-point boundary condition and standard θ-schemes) are well known, and we do not claim novelty for any of them separately. Table 1 compares the method with the closest front-fixing finite difference schemes. Wu and Kwok [28] introduced the logarithmic variable $x = \ln(S/S_f)$ for the American put. Nielsen et al. [21] used $x = S/S_f$, approximated the transport term containing S_f' by central differences with a difference quotient of S_f, computed the boundary in their explicit scheme from a closed-form expression and in their implicit scheme by Newton's method for the coupled system; for the front-fixing schemes their support is numerical (their stability and positivity results concern the penalty method). Company et al. [5] analysed an explicit scheme in the logarithmic variable, in which the boundary is obtained without iteration, and

Corrected Proof

proved positivity, monotonicity, consistency and a conditional stability result for a linearised model. Fazio et al. [10] used a fully implicit scheme, solved the nonlinear system for the option values and the boundary at every step, and studied stability by a frozen-coefficient von Neumann analysis. In all of these schemes the velocity term is approximated on the fixed x-grid by a difference quotient of S_f (an Eulerian treatment). The contributions of the present paper relative to [5, 10, 21] are: (i) the treatment of the velocity term along the characteristics $S = \text{const}$ (Section 3.1), which leaves an operator with constant coefficients and, as shown in Remark 4 and Table 11, avoids the spurious boundary root that the Eulerian treatment produces for the fully implicit scheme; (ii) the boundary update (U1), which imposes the curvature condition of Lemma 1 at a ghost point (we are not aware of an earlier use of this condition in a boundary update), solved as a bracketed scalar equation (Section 3.3); (iii) for a prescribed boundary position, an analysis of the linear steps: stability of the linear diffusion update of all three θ-schemes for the actual constant-coefficient operators, without freezing coefficients (Theorems 1-3), and, for the transfer, a one-step interpolation estimate whose constant does not depend on the shift or the mesh size (Proposition 1) together with an analytic proof of the von Neumann stability of a single transfer step (Lemma 3); and (iv) a comparison with independent references, in particular an integral-equation solution for the exercise boundary, together with a quantification of the projection error of the fixed-grid Crank-Nicolson scheme. As for the schemes in [5, 10, 21], no stability or convergence theorem is proved for the fully coupled nonlinear scheme (Remark 3 and Section 4.3); the results in (iii) are statements about single linear steps and do not imply such a theorem.

Table 1: Comparison with the closest front-fixing finite difference schemes for the American put

	Nielsen et al. [21]	Company et al. [5]	Fazio et al. [10]	present paper
variable	$x = S/S_f$	$x = \ln(S/S_f)$	$x = \ln(S/S_f)$	$x = \ln(S/S_f)$, grid moving with S_f
time stepping	explicit; implicit	explicit	implicit	θ-scheme, $\theta = 0, 1, \frac{1}{2}$
velocity term	difference quotient of S_f (Eulerian)	difference quotient of S_f (Eulerian)	difference quotient of S_f (Eulerian)	along characteristics $S = \text{const}$ (cubic transfer)
boundary	closed form (explicit); Newton for the coupled system (implicit)	closed form, no iteration	coupled nonlinear system	scalar equation (26) with curvature-based update (U1), bracketed Brent solver
stability analysis	numerical only (for front fixing)	positivity, monotonicity; conditional stability of a linearised model	frozen-coefficient von Neumann	linear steps only, prescribed boundary: exact von Neumann and Dirichlet-matrix analysis of the diffusion step; maximum principle; one-step transfer estimate; transfer stability
stability and convergence of the coupled scheme	not proved	not proved	not proved	not proved; errors against independent references observed

In recent years, neural network-based methods have received increasing attention for solving option pricing problems; for early exercise see, e.g., Gatta et al. ([13]) and, for a time-fractional model, Nuugulu et al. ([22]). These approaches approximate option values by learning mappings between financial variables, such as asset prices, volatility, interest rates, and maturity, through network training. However, their application to American options remains challenging due to the unknown exercise boundary and the non-smooth behaviour of option values near this boundary. Furthermore, neural networks require large and reliable datasets, which may be difficult to obtain from financial markets due to noise, missing observations, and other imperfections. When real data are unavailable, synthetic datasets generated using methods such as Monte Carlo simulations are often employed, but the quality of such data directly affects model performance.

Monte Carlo methods have also been widely used in option pricing, for American options in particular by Longstaff and Schwartz ([19]) and Maidoumi et al. ([20]); American options under stochastic volatility with double exponential jumps are studied by Fallah and Mehrdoust ([9]). Although flexible, their application to American options requires additional procedures to determine the optimal exercise

Corrected Proof

strategy by comparing immediate exercise payoff with continuation value. Regression-based approaches, such as Longstaff and Schwartz ([19]), approximate the continuation value but introduce additional complexity and possible errors in identifying the exercise boundary. Operator splitting methods, including those proposed by Ikonen and Toivanen ([14, 15]), provide alternative frameworks by decomposing the free boundary problem into simpler sub-problems. However, these approaches often require iterative boundary updates, increasing computational cost and implementation complexity. These limitations motivate the continued use of finite difference methods for American option pricing, particularly for low-dimensional problems involving free boundaries.

On the empirical side, the inputs of the model have to be estimated from market data. Here we explain how this is done: the volatilities are historical (close-to-close) volatilities of daily log-returns, which we compare with range-based estimators [12, 23, 26, 29], and the risk-free rate is the policy repo rate of the Reserve Bank of India [25]. We also quantify how sensitive the computed prices and exercise boundaries are to these inputs, to the choice of the free-boundary update, and to the moneyness of the option, and we explain how the non-smoothness of the payoff at the strike is handled. Since exchange-traded single-stock options in India are European-style, the numerical study is a model-parameter study: it values hypothetical American puts written on the four bank stocks, with parameters estimated from historical stock prices and with dividends omitted (the effect of a dividend yield is quantified in Section 5.1). It is not an empirical validation against prices of traded American options. The underlying data are unadjusted daily closing prices from the National Stock Exchange of India; all eight series are supplied as a supplementary workbook (Section 5).

The remainder of this paper is organized as follows. In Section 2, we introduce the mathematical formulation of the American put option pricing problem, including its front-tracking (transformed) form. The numerical schemes developed for solving the resulting problem are presented in Section 3, followed by an analysis of the linear steps (local consistency, stability of the diffusion update and the interpolation transfer, for a prescribed boundary position) in Section 4. In Section 5, we present comparative numerical experiments, an error study against independent reference solutions, a sensitivity analysis, and an application of the proposed methodology to real financial data from the Indian market involving two public sector and two private sector banks. Finally, in Section 6, we summarize the main findings of the paper and discuss possible directions for future research.

2 Mathematical model

Consider the Black-Scholes partial differential equation describing the value of an American put option

$$\begin{cases} \dfrac{\partial V}{\partial t}+\dfrac{1}{2}\sigma^2 S^2\dfrac{\partial^2 V}{\partial S^2}+rS\dfrac{\partial V}{\partial S}-rV=0,\ S>\bar{S}_f(t),\ 0\le t<T \\ V(S,T)=\max(K-S,0),\ S\ge 0, \\ \dfrac{\partial V}{\partial S}(\bar{S}_f(t),t)=-1,\ V(\bar{S}_f(t),t)=K-\bar{S}_f(t),\ \lim\limits_{S\to\infty}V(S,t)=0, \\ V(S,t)=K-S,\ 0\le S<\bar{S}_f(t), \end{cases} \tag{1}$$

where $\bar{S}_f(t)$ represents the free (and moving) boundary in calendar time t. Since early exercise is permitted, the value V of the option satisfies

$$V(S,t)\ge \max(K-S,0), \quad S\ge 0,\ 0\le t\le T. \tag{2}$$

Corrected Proof

In the above S denotes the market price of the underlying asset, σ is the volatility of the underlying asset, K is the exercise price, T is the expiry time, and r is the risk-free interest rate. In fact, due to early exercise features, an equivalent representation of (1) would be a partial differential inequality of the form

$$\frac{\partial V}{\partial t} + \frac{1}{2}\sigma^2 S^2 \frac{\partial^2 V}{\partial S^2} + rS\frac{\partial V}{\partial S} - rV \leq 0, \tag{3}$$

$$V(S,t) \geq \max(K-S,0), \ \ \forall\, t \in [0,T], \ \ S \geq 0. \tag{4}$$

Hence, at any point (S,t) it will be optimal to either exercise or hold on to the option and hence for each S, t, one of the above two inequalities would actually be an equality. This constitutes the American option valuation as a linear complementarity problem:

$$\left(\frac{\partial V}{\partial t} + \mathscr{L}_{BS}V\right)(V-g) = 0, \quad \frac{\partial V}{\partial t} + \mathscr{L}_{BS}V \leq 0, \quad V - g \geq 0, \tag{5}$$

where $\mathscr{L}_{BS}V = \frac{1}{2}\sigma^2 S^2 V_{SS} + rSV_S - rV$ and $g(S) = \max(K-S,0)$. The resulting problem can be solved either on a fixed grid as a (discrete) complementarity problem, or by keeping the free boundary as an unknown and transforming the continuation region onto a fixed domain. We follow the second approach, and use the first one for comparison (Section 3.4).

Boundary behaviour at $S = 0$. For $0 \leq S < \bar{S}_f(t)$ the last condition in (1) gives $V(S,t) = K - S$; in particular $V(0,t) = K \quad \forall\, 0 \leq t \leq T$, since it is optimal to exercise a put immediately when the asset is worthless. Moreover, $V(S,t) \approx 0, \quad$ for large S.

2.1 Front-tracking formulation

We first convert the final value problem into an initial value problem by the change of variables $\tau = T - t$ (time to expiry) . We keep the notation $V(S,\tau)$ for the option value and denote the boundary in time to expiry by

$$S_f(\tau) := \bar{S}_f(T-\tau), \qquad 0 \leq \tau \leq T. \tag{6}$$

Thus $S_f(0) = \bar{S}_f(T) = K$ is the boundary at expiry, and $S_f(T) = \bar{S}_f(0)$ is the boundary at the valuation date $t = 0$. From here on only the time-to-expiry notation $S_f(\tau)$ is used; all exercise boundaries reported in Section 5 are the values $S_f(T)$ at the valuation date, approximated by the last computed value $S_f^N \approx S_f(\tau_N) = S_f(T)$, and the boundaries in Figure 4 are plotted against τ. Problem (1) becomes

$$\begin{aligned}
&\frac{\partial V}{\partial \tau} = \frac{1}{2}\sigma^2 S^2 \frac{\partial^2 V}{\partial S^2} + rS\frac{\partial V}{\partial S} - rV, \qquad S > S_f(\tau),\ 0 < \tau \leq T, \\
&V(S,0) = \max(K-S,0), \qquad S_f(0) = K, \\
&V(S_f(\tau),\tau) = K - S_f(\tau), \qquad \frac{\partial V}{\partial S}(S_f(\tau),\tau) = -1, \qquad \lim_{S\to\infty} V(S,\tau) = 0,
\end{aligned} \tag{7}$$

and $V(S,\tau) = K - S$ for $0 \leq S \leq S_f(\tau)$. The initial position $S_f(0) = K$ holds for a put on a non-dividend-paying asset.

Corrected Proof

Transformation. Following [5], we introduce

$$x = \ln \frac{S}{S_f(\tau)}, \qquad u(x,\tau) = V\big(S_f(\tau)e^x, \tau\big), \qquad s(\tau) = \frac{S_f'(\tau)}{S_f(\tau)} = \frac{d}{d\tau}\ln S_f(\tau). \tag{8}$$

The continuation region $S > S_f(\tau)$ is mapped onto the fixed half-line $x > 0$ and the free boundary onto $x = 0$. By the chain rule,

$$S\frac{\partial V}{\partial S} = \frac{\partial u}{\partial x}, \qquad S^2\frac{\partial^2 V}{\partial S^2} = \frac{\partial^2 u}{\partial x^2} - \frac{\partial u}{\partial x}, \qquad \frac{\partial V}{\partial \tau}\Big|_S = \frac{\partial u}{\partial \tau} + \frac{\partial u}{\partial x}\frac{\partial x}{\partial \tau}\Big|_S = \frac{\partial u}{\partial \tau} - s(\tau)\frac{\partial u}{\partial x}.$$

Substituting into (7) gives the transformed problem

$$\frac{\partial u}{\partial \tau} = \frac{1}{2}\sigma^2\frac{\partial^2 u}{\partial x^2} + \Big(r - \frac{\sigma^2}{2} + \frac{S_f'(\tau)}{S_f(\tau)}\Big)\frac{\partial u}{\partial x} - ru, \qquad x > 0,\ 0 < \tau \le T, \tag{9}$$

$$u(0,\tau) = K - S_f(\tau), \qquad \frac{\partial u}{\partial x}(0,\tau) = -S_f(\tau),\ \lim_{x\to\infty} u(x,\tau) = 0,\ u(x,0) = 0\ (x>0),\ S_f(0) = K. \tag{10}$$

The value-matching and smooth-pasting conditions have become two boundary conditions at $x = 0$ for a second-order equation; the extra condition determines the unknown $S_f(\tau)$. The only non-constant coefficient of (9) is the boundary velocity $s(\tau) = S_f'/S_f$, which does not depend on x.

Lemma 1 (Curvature condition at the free boundary)**.** *If u is smooth up to $x = 0$ for $\tau > 0$, then*

$$\frac{\partial^2 u}{\partial x^2}(0,\tau) = \frac{2rK}{\sigma^2} - S_f(\tau), \qquad \textit{equivalently} \qquad \frac{1}{2}\sigma^2 S_f^2\frac{\partial^2 V}{\partial S^2}(S_f^+,\tau) = rK. \tag{11}$$

Proof. Differentiating the value-matching condition in τ gives $u_\tau(0,\tau) = -S_f'(\tau) = -s(\tau)S_f(\tau)$. Evaluating (9) at $x = 0$ and using $u(0,\tau) = K - S_f$, $u_x(0,\tau) = -S_f$,

$$-sS_f = \tfrac{1}{2}\sigma^2 u_{xx}(0,\tau) - \big(r - \tfrac{\sigma^2}{2} + s\big)S_f - r(K - S_f) = \tfrac{1}{2}\sigma^2 u_{xx}(0,\tau) + \tfrac{\sigma^2}{2}S_f - sS_f - rK,$$

and the terms $-sS_f$ cancel. The second form follows from $S^2V_{SS} = u_{xx} - u_x$. □

Behaviour near expiry. Close to expiry the exercise boundary behaves like $S_f(\tau) \sim K\big(1 - \sigma\sqrt{\tau|\ln\tau|}\big)$ as $\tau \to 0^+$ [1]. Consequently $s(\tau)$ is unbounded as $\tau \to 0^+$, and u is not smooth at $(x,\tau) = (0,0)$; this is how the kink of the payoff at $S = K$ manifests itself in the transformed variables (see Section 5.10). The initial function $u(x,0) = 0$ itself is smooth.

Domain truncation. For computations the half-line is truncated to $[0, x_{\max}]$ with $u(x_{\max},\tau) = 0$. With $x_{\max} = 1.5$ the computational domain extends to $S = S_f(\tau)e^{1.5} \approx 4.48\,S_f(\tau)$; the influence of this choice is examined in Section 5.9. The truncation condition replaces the exact value $u(x_{\max},\tau) = V(S_f(\tau)e^{x_{\max}},\tau) > 0$ by zero. Since V is increasing in τ and decreasing in S, and S_f is decreasing in τ, the largest value replaced in this way is

$$\varepsilon_{\mathrm{tr}} := \max_{0\le\tau\le T} V\big(S_f(\tau)e^{x_{\max}},\tau\big) = V\big(S_f(T)e^{x_{\max}},T\big). \tag{12}$$

Corrected Proof

The solution V^{tr} of the truncated problem, with exercise boundary S_f^{tr}, is the value of an American put that is cancelled without payment when S reaches the moving barrier $B(\tau) = S_f^{\mathrm{tr}}(\tau)e^{x_{\max}}$. Hence $V^{\mathrm{tr}} \le V$, so that $S_f^{\mathrm{tr}} \ge S_f$ and $B(\tau) \ge S_f(\tau)e^{x_{\max}}$, and the strong Markov property (stopping at the first time at which the barrier is reached) gives

$$0 \le V(S,\tau) - V^{\mathrm{tr}}(S,\tau) \le \varepsilon_{\mathrm{tr}}. \tag{13}$$

For the eight data sets of Section 5, $\varepsilon_{\mathrm{tr}}$ lies between $3\times10^{-42}K$ and $3.5\times10^{-8}K$ (Table 20).

Remark 1 (Front fixing and front tracking)**.** *In the variable x the free boundary is fixed at $x = 0$ (a Landau, or front-fixing, transformation). In the original variables the grid points $S_j(\tau) = S_f(\tau)e^{x_j}$ move with the free boundary, which is computed together with the solution at every time level; in this sense the method tracks the front. Throughout the paper,* front fixing *refers only to the change of variables, as in [5, 10, 21], and* front tracking *to the complete method (transformation, moving grid, transfer and boundary update). The fixed-grid approach of Brennan and Schwartz [2] is different: there the boundary is not an unknown but is identified a posteriori from the solution of a discrete complementarity problem (Section 3.4).*

3 Derivation of the numerical methods

Let $x_j = j\Delta x$, $j = 0,1,\dots,M$, $\Delta x = x_{\max}/M$, and let $0 = \tau_0 < \tau_1 < \cdots < \tau_N = T$ with $\Delta\tau_n = \tau_{n+1} - \tau_n$. Unless stated otherwise we use the graded mesh

$$\tau_n = T\left(\frac{n}{N}\right)^2, \qquad n = 0,1,\dots,N, \tag{14}$$

which concentrates time steps near expiry, where $s(\tau)$ is singular (a uniform mesh, $\tau_n = nT/N$, is used for comparison). We denote by $U_j^n \approx u(x_j,\tau_n)$ and $S_f^n \approx S_f(\tau_n)$ the discrete unknowns; the corresponding asset prices $S_j^n = S_f^n e^{x_j}$ form a grid which moves with the free boundary. Since $S_f(\tau)$ is decreasing, $\delta_n := \ln(S_f^{n+1}/S_f^n) \le 0$.

3.1 Treatment of the velocity term: characteristics

The derivation of (9) shows that the velocity term only expresses the fact that the grid moves: along a line $S = \text{const}$ the time derivative is $\partial_\tau V|_S = u_\tau - s\,u_x$, and there (9) reduces to

$$\frac{\partial V}{\partial\tau}\Big|_S = \mathscr{L}u, \qquad \mathscr{L}u := \frac{1}{2}\sigma^2 u_{xx} + \mu\,u_x - ru, \qquad \mu := r - \frac{\sigma^2}{2}, \tag{15}$$

an operator with constant coefficients. We therefore discretise the time derivative along the lines $S = S_j^{n+1}$ through the nodes of the new grid (a characteristic, or semi-Lagrangian, treatment of $s\,u_x$ [8]). This requires the old solution at the new nodes,

$$\widetilde{U}_j^n \approx V(S_j^{n+1},\tau_n) = u(x_j+\delta_n,\tau_n), \qquad j = 0,1,\dots,M. \tag{16}$$

If $x_j + \delta_n < 0$, the node S_j^{n+1} lies in the exercise region at time τ_n and $\widetilde{U}_j^n = K - S_j^{n+1}$ exactly. Otherwise $\widetilde{U}_j^n$ is obtained by cubic Lagrange interpolation of U^n at the point $x_j + \delta_n$; for stencils reaching beyond

Corrected Proof

$x = 0$ the data are continued by the Taylor polynomial $K - S_f^n - S_f^n x + (rK/\sigma^2 - S_f^n/2)x^2$, which by (10) and Lemma 1 matches u, u_x and u_{xx} at the front. We write $\widetilde{U}^n = \Pi_n U^n$. The stencil always consists of the four nodes surrounding the foot $x_j + \delta_n$ of the characteristic, which may lie several cells away from x_j (this happens in the first steps of coarse time meshes, see Section 5.2.1); no restriction on $|\delta_n|/\Delta x$ is required (Proposition 1 and Lemma 3). More precisely, for a foot $y = x_j + \delta_n \geq 0$ let $k = \lfloor y/\Delta x \rfloor$ and $\vartheta = y/\Delta x - k \in [0,1)$; the stencil is $\{x_{k-1}, x_k, x_{k+1}, x_{k+2}\}$ and $\widetilde{U}_j^n = \sum_{i=-1}^{2} w_i(\vartheta) U_{k+i}^n$ with the cubic Lagrange weights w_i of Lemma 3. A foot that coincides with a node ($\vartheta = 0$) returns the nodal value. Since $\delta_n \leq 0$, the foot of every interior node satisfies $y \leq x_{M-1}$, hence $0 \leq k \leq M-2$ and the stencil lies in $[x_{-1}, x_M]$: at the left end the ghost value U_{-1}^n is the Taylor value just described ($k = 0$, at most one node per step), and at the right end the value $U_M^n = 0$ of the truncated problem enters the stencils of the feet in $[x_{M-2}, x_{M-1}]$. No one-sided or extrapolating stencil is used for the interior nodes. For $j = M$ the transferred value is not used: it is overwritten by the truncation condition $\widetilde{U}_M^n = 0$ in (19). At the truncated endpoint $x_M = x_{\max}$ three values have to be distinguished: (a) the value imposed by the truncation condition, $\widetilde{U}_M^n = U_M^{n+1} = 0$; (b) the interpolated value $(\Pi_n U^n)_M$ at the foot $x_M + \delta_n < x_{\max}$, which is computed only for monitoring (with the stencil $x_{M-3}, \ldots, x_M$, the only place where the stencil is not centred on the cell of the foot) and then discarded; and (c) the exact value $u(x_M + \delta_n, \tau_n) = V(S_M^{n+1}, \tau_n)$. The scheme uses (a). Value (b) is not an approximation of (c): it is interpolated from data that already satisfy $U_M^n = 0$, so that it is of the size $|\delta_n|\,|U_{M-1}^n|/\Delta x$ of a computed quantity of the truncated problem; in all computations of Section 5 it was below $10^{-9}K$ (Table 20). The difference between (a) and (c) is the error of the truncation condition itself; it is bounded by $\varepsilon_{\mathrm{tr}}$ in (12)-(13). Neither difference enters the consistency analysis of Section 4, which concerns the interior nodes $j = 1, \ldots, M-1$; their effect on the reported prices and exercise boundaries is quantified in Section 5.9 (Table 20). Since $u(x_j + \delta_n, \tau_n) = u(x_j, \tau_n) + \delta_n u_x + O(\delta_n^2)$ and $\delta_n = s(\tau_n)\Delta\tau_n + O(\Delta\tau_n^2)$,

$$\frac{u(x_j, \tau_{n+1}) - u(x_j + \delta_n, \tau_n)}{\Delta\tau_n} = u_\tau - s\,u_x + O(\Delta\tau_n),$$

so that the transfer step is precisely the discrete counterpart of the term $-\frac{S_f'}{S_f} u_x$ in (9). The exact treatment of this term is essential: a direct (Eulerian) central-difference approximation of $s\,u_x$ with $s^{n+1/2} = \delta_n/\Delta\tau_n$ works for the explicit and Crank-Nicolson schemes on fine grids, but for the fully implicit scheme the grid Péclet number $|s|\Delta x/\sigma^2$ is very large in the first time steps and the discrete boundary equation acquires a spurious root (Remark 4 and Table 11).

3.2 The three finite difference schemes

With the standard second-order central differences, $\mathscr{L}$ is approximated at the interior nodes by

$$(AU)_j = aU_{j-1} + bU_j + cU_{j+1}, \qquad a = \frac{\sigma^2}{2\Delta x^2} - \frac{\mu}{2\Delta x}, \quad b = -\frac{\sigma^2}{\Delta x^2} - r, \quad c = \frac{\sigma^2}{2\Delta x^2} + \frac{\mu}{2\Delta x}, \tag{17}$$

$j = 1, \ldots, M-1$. For $\theta \in [0,1]$ the θ-scheme reads

$$\frac{U_j^{n+1} - \widetilde{U}_j^n}{\Delta\tau_n} = \theta\,(AU^{n+1})_j + (1-\theta)(A\widetilde{U}^n)_j, \qquad j = 1, \ldots, M-1, \tag{18}$$

Corrected Proof

with the boundary values

$$U_0^{n+1} = \widetilde{U}_0^n = K - S_f^{n+1}, \qquad U_M^{n+1} = \widetilde{U}_M^n = 0. \tag{19}$$

The choice $\theta = 0$ gives the explicit (forward-time central-space) finite difference method (EFDM), $\theta = 1$ the fully implicit (backward-time central-space) method (IFDM), and $\theta = \frac{1}{2}$ the Crank-Nicolson method (CNM). In matrix form, with $\mathbf{U}^n = (U_1^n, \dots, U_{M-1}^n)^\top$ and the $(M-1)\times(M-1)$ matrices $T_1 = \text{tridiag}(-1,0,1)$ and $T_2 = \text{tridiag}(1,-2,1)$, we have

$$A = \frac{\sigma^2}{2\Delta x^2} T_2 + \frac{\mu}{2\Delta x} T_1 - rI, \tag{20}$$

and the three schemes are

$$\text{EFDM:} \quad \mathbf{U}^{n+1} = F_n \widetilde{\mathbf{U}}^n + \mathbf{p}^n, \qquad F_n = I + \Delta\tau_n A, \tag{21}$$

$$\text{IFDM:} \quad B_n \mathbf{U}^{n+1} = \widetilde{\mathbf{U}}^n + \mathbf{q}^n, \qquad B_n = I - \Delta\tau_n A, \tag{22}$$

$$\text{CNM:} \quad \Big(I - \frac{\Delta\tau_n}{2} A\Big)\mathbf{U}^{n+1} = \Big(I + \frac{\Delta\tau_n}{2} A\Big)\widetilde{\mathbf{U}}^n + \frac{1}{2}\big(\mathbf{p}^n + \mathbf{q}^n\big), \tag{23}$$

where $\mathbf{p}^n = \mathbf{q}^n = \Delta\tau_n\, a\,(K - S_f^{n+1})\,\mathbf{e}_1$ carry the boundary value at $x = 0$ ($\mathbf{e}_1$ is the first unit vector; the contribution of $U_M = 0$ vanishes). The coefficients of A are constant (they no longer depend on j), the sign conventions of the explicit and implicit matrices are consistent, and the Crank-Nicolson method is the genuine $\theta = \frac{1}{2}$ scheme rather than an average of the other two.

3.3 The free-boundary update equation

The unknown S_f^{n+1} is determined by the smooth-pasting condition. Introducing a ghost value U_{-1} and approximating $u_x(0,\tau) = -S_f$ and $u_{xx}(0,\tau) = 2rK/\sigma^2 - S_f$ (Lemma 1) by central differences,

$$\frac{U_1 - U_{-1}}{2\Delta x} = -S_f, \qquad \frac{U_1 - 2U_0 + U_{-1}}{\Delta x^2} = \frac{2rK}{\sigma^2} - S_f, \qquad U_0 = K - S_f,$$

and eliminating U_{-1}, we obtain gives the boundary-update equation

$$\text{(U1)} \quad S_f^{n+1} = \frac{K\big(1 + r\Delta x^2/\sigma^2\big) - U_1^{n+1}}{1 + \Delta x + \Delta x^2/2}. \tag{24}$$

A Taylor expansion of the exact solution, $u(\Delta x,\tau) = u(0,\tau) + \Delta x\, u_x + \frac{\Delta x^2}{2} u_{xx} + \frac{\Delta x^3}{6} u_{xxx} + O(\Delta x^4)$, shows that (24) is satisfied by (u, S_f) up to a defect $\frac{\Delta x^3}{6} u_{xxx}(0,\tau) + O(\Delta x^4)$. For the sensitivity analysis of Section 5.8, we also consider two updates based on one-sided approximations of $u_x(0,\tau) = -S_f$ alone:

$$\text{(U2)} \quad S_f^{n+1} = \frac{3K - 4U_1^{n+1} + U_2^{n+1}}{3 + 2\Delta x}, \qquad \text{(U3)} \quad S_f^{n+1} = \frac{K - U_1^{n+1}}{1 + \Delta x}, \tag{25}$$

which are of second and first order, respectively.

Solution of the coupled problem. For a trial value S of S_f^{n+1} let $\Phi_n(S)$ be the value obtained by three

Corrected Proof

operations: the transfer (16) with the shift $\delta = \ln(S/S_f^n)$, the θ-step (18)-(19) with the boundary value $U_0^{n+1} = K - S$, and the update (24) applied to the resulting U_1^{n+1}. The new boundary is a root of the residual equation

$$F_n(S) := S - \Phi_n(S) = 0, \qquad S \in \mathscr{I}_n := (0, S_f^n]. \tag{26}$$

The admissible interval $\mathscr{I}_n$ expresses the positivity of the boundary and the monotonicity $S_f^{n+1} \le S_f^n$; the transfer also requires $\delta \le 0$. The root is computed in three stages (Sg):

(Sg 1) *Upper end.* $F_n(S_f^n)$ is evaluated. If $F_n(S_f^n) = 0$, then $S_f^{n+1} = S_f^n$ is accepted; if $F_n(S_f^n) < 0$, the computation stops with an error message (failure of type 1).

(Sg 2) *Bracket.* With $d_0 = \Delta x S_f^n$, the points $a_k = S_f^n - 2^k d_0$, $k = 0, 1, \ldots$, are tried in turn; as long as $F_n(a_k) > 0$, the upper end of the bracket is moved to a_k and k is increased. The first a_k with $F_n(a_k) \le 0$ becomes the lower end. Positivity is enforced: if $a_k \le 0$, or if more than 60 expansions would be needed, the computation stops with an error message (failure of type 2). Hence the bracket always lies in $\mathscr{I}_n$.

(Sg 3) *Brent's method* [3] (safeguarded secant, inverse quadratic interpolation and bisection), which never leaves the bracket. The iteration stops when the half-width of the current bracket $[b, c]$ (with $F_n(b)F_n(c) \le 0$) satisfies $\frac{1}{2}|c - b| \le 2\varepsilon_{\text{mach}}|b| + \frac{1}{2}\,\text{tol}$, $\text{tol} = 10^{-12}K$, or when $F_n(b) = 0$ in floating point arithmetic; the accepted value is the end point b with the smaller $|F_n|$. If 100 iterations do not suffice, the computation stops with an error message (failure of type 3).

There is no fallback: a failure of any type terminates the computation, so that every reported result was obtained with a root that satisfies the stopping rule. The residual $|F_n|$ at the accepted root, the number of expansions in (Sg 2) and the number of Brent iterations are recorded at every step. The procedure returns one root, in the first bracket in which a sign change is found; it does not by itself detect further roots in $\mathscr{I}_n$, and this was checked separately by tabulating F_n. The numbers of computations, steps, evaluations and failures (none) for all computations of the paper are reported in Section 5.6.1. The bracketing is important: away from the root F_n is almost constant (the solution is then locally close to the payoff), and unsafeguarded secant or fixed-point iterations may leave the admissible interval. Each evaluation of Φ_n costs one tridiagonal solve, and on average 6.6-7.1 evaluations per time step are needed for $M = N = 400$ (6.3 over all computations of the paper) (including those for the bracket). We do not have a general existence or uniqueness result for the root of (26); the checks of Section 5.6.1 are numerical evidence for the tested parameter sets only, not a proof of existence or uniqueness.

3.4 Fixed-grid discrete complementarity formulation

For comparison we also solve (5) directly on a fixed uniform grid $S_j = jh$, $h = S_{\max}/M$, $S_{\max} = 4K$, with the correct boundary values $V_0 = K$ and $V_M = 0$. Let A_h be the central-difference approximation of $\mathscr{L}_{BS}$, i.e., $(A_h V)_j = \alpha_j V_{j-1} + \beta_j V_j + \gamma_j V_{j+1}$ with $\alpha_j = \frac{1}{2}(\sigma^2 j^2 - rj)$, $\beta_j = -(\sigma^2 j^2 + r)$, $\gamma_j = \frac{1}{2}(\sigma^2 j^2 + rj)$, and let $g_j = \max(K - S_j, 0)$. The θ-scheme leads at every time level to the discrete linear complementarity problem

$$\mathscr{A}\mathbf{V}^{n+1} - \mathbf{b}^n \ge 0, \qquad \mathbf{V}^{n+1} - \mathbf{g} \ge 0, \qquad \left(\mathscr{A}\mathbf{V}^{n+1} - \mathbf{b}^n\right)^\top \left(\mathbf{V}^{n+1} - \mathbf{g}\right) = 0, \tag{27}$$

with $\mathscr{A} = I - \theta\Delta\tau_n A_h$ and $\mathbf{b}^n = (I + (1-\theta)\Delta\tau_n A_h)\mathbf{V}^n$ plus boundary terms. For the put, (27) is solved exactly by the Brennan-Schwartz algorithm [2, 16]: a Gaussian elimination of the tridiagonal matrix

Corrected Proof

from the row of largest S downwards, followed by a substitution from small S upwards in which $V_j = \max\{g_j, (y_j - \alpha'_j V_{j-1})/d_j\}$ is applied row by row. In contrast, the frequently used projection $\mathbf{V}^{n+1} = \max(\mathscr{A}^{-1}\mathbf{b}^n, \mathbf{g})$ solves the unconstrained system first and applies the constraint afterwards. For $\theta = 0$ ($\mathscr{A} = I$) both coincide, but for $\theta > 0$ the projection is an operator-splitting approximation of (27) with a splitting error of order $O(\Delta\tau)$ [14]. The effect of the projection method is quantified in Table 10.

4 Analysis of the linear steps of the numerical methods

One time step of the method consists of three parts, which are analysed separately: (L1) the *linear diffusion update* (18)-(19) for a prescribed boundary position S_f^{n+1} and prescribed transferred data $\widetilde{U}^n$; (L2) the *interpolation transfer* Π_n for a prescribed shift δ_n; and (L3) the *fully coupled nonlinear procedure*, in which S_f^{n+1}, and hence δ_n, are determined by the residual equation (26). This section proves local consistency of the linear step (Section 4.1), stability of (L1) (Theorems 1-3), a one-step error estimate for (L2) (Proposition 1) and the von Neumann stability of a single application of (L2) (Lemma 3). These are statements about single linear steps. For (L3) no existence, uniqueness, stability or convergence result is proved; its behaviour is assessed numerically in Section 5 (see Section 4.3).

4.1 Local consistency of the linear step

Let u be a smooth solution of (9)-(10) on $[0, x_{\max}] \times [\tau_n, \tau_{n+1}]$ and let $u_j^n = u(x_j, \tau_n)$. Taylor expansion about x_j gives

$$(Au)_j = \mathscr{L}u(x_j) + \Delta x^2 \Big(\frac{\sigma^2}{24} \frac{\partial^4 u}{\partial x^4} + \frac{\mu}{6} \frac{\partial^3 u}{\partial x^3} \Big)(x_j) + O(\Delta x^4). \tag{28}$$

Next, we fix the grid of level $n+1$ and let $w_j(\tau) = V(S_j^{n+1}, \tau)$ be the exact value along the line $S = S_j^{n+1}$. By (15), $w_j' = \mathscr{L}\hat{u}(x_j, \tau)$, where $\hat{u}(y, \tau) = V(S_f^{n+1} e^y, \tau)$, and $w_j(\tau_{n+1}) = u_j^{n+1}$, $w_j(\tau_n) = u(x_j + \delta_n, \tau_n)$. The local truncation error of (18),

$$R_j^n := \frac{u_j^{n+1} - (\Pi_n u^n)_j}{\Delta\tau_n} - \theta (Au^{n+1})_j - (1-\theta)(A\Pi_n u^n)_j,$$

therefore consists of three parts: the usual θ-method error in time, $\big(\frac{1}{2} - \theta\big)\Delta\tau_n w_j''(\tau_{n+1/2}) + O(\Delta\tau_n^2)$; the spatial error (28); and the interpolation error of the transfer divided by $\Delta\tau_n$. For the last part we use the following estimate, which holds for shifts of any size.

Proposition 1 (One-step interpolation error for arbitrary shifts)**.** *Assume: (A1) the grid is uniform, $x_i = i\Delta x$, $i = -1, 0, \ldots, M$, $\Delta x = x_{\max}/M$, $M \geq 3$; (A2) the interpolation point y lies in the cell $[x_k, x_{k+1}]$ with $0 \leq k \leq M-2$, $\vartheta = (y - x_k)/\Delta x \in [0,1]$, and $p(y) = \sum_{i=-1}^{2} w_i(\vartheta) v(x_{k+i})$ is the value at y of the cubic polynomial interpolating v at $x_{k-1}, \ldots, x_{k+2}$, with the Lagrange weights w_i of Lemma 3; (A3) $y = x_j + \delta$ for a grid point x_j and a shift δ of arbitrary size; (A4) $v \in C^4[x_{k-1}, x_{k+2}]$ (for $k = 0$, v is a C^4 extension to $[-\Delta x, x_{\max}]$ of a function defined on $[0, x_{\max}]$). Then*

$$|v(y) - p(y)| \leq \frac{3}{32}\, \vartheta(1-\vartheta)\, \Delta x^4\, \|v''''\|_{\infty, [x_{k-1}, x_{k+2}]}, \tag{29}$$

Corrected Proof

and the constant $\frac{3}{32}$ *is sharp. Consequently,*

$$|v(y)-p(y)| \le \frac{3}{32}\min\Big(\frac{|\delta|}{\Delta x},\frac{1}{4}\Big)\Delta x^4\,\|v''''\|_\infty, \tag{30}$$

without any restriction on $|\delta|/\Delta x$*; the constants do not depend on* k*,* j*,* δ*,* Δx *or* M*. If the stencil contains* x_{-1} *(i.e.,* $k=0$*) and the value at* x_{-1} *is replaced by* $P(-\Delta x)$*, where the quadratic* P *matches* v*,* v' *and* v'' *at* $x=0$*, then an additional error of at most* $\frac{1}{18}|\delta|\,\Delta x^2\,\|v'''\|_{\infty,[-\Delta x,0]}$ *occurs.*

Proof. Since the weights reproduce polynomials of degree three, $\sum_i w_i(\vartheta)=1$ and $\sum_i w_i(\vartheta)(i-\vartheta)^m=0$ for $m=1,2,3$; hence the error functional $v\mapsto v(y)-p(y)$ annihilates cubics, and the Lagrange (Cauchy) form of the remainder gives

$$v(y)-p(y)=\frac{v''''(\xi)}{24}\prod_{i=-1}^{2}(y-x_{k+i}),\qquad \Big|\prod_{i=-1}^{2}(y-x_{k+i})\Big|=\vartheta(1-\vartheta)(1+\vartheta)(2-\vartheta)\Delta x^4,$$

with $\xi\in(x_{k-1},x_{k+2})$. Because $(1+\vartheta)(2-\vartheta)=2+\vartheta(1-\vartheta)\le\frac{9}{4}$, with equality at $\vartheta=\frac{1}{2}$, (29) follows, with equality for $v(x)=x^4$ and $\vartheta=\frac{1}{2}$. Since x_j is a grid point at distance $|\delta|$ from y, the distance from y to the nearest grid point, $\min(\vartheta,1-\vartheta)\Delta x$, is at most $|\delta|$, and $\vartheta(1-\vartheta)\le\min(\vartheta,1-\vartheta)\le|\delta|/\Delta x$; together with $\vartheta(1-\vartheta)\le\frac{1}{4}$ this gives (30). Finally, with the ghost value the interpolant becomes $\tilde p(y)=p(y)+w_{-1}(\vartheta)\big(P(-\Delta x)-v(-\Delta x)\big)$, where the weight of x_{-1} is $w_{-1}(\vartheta)=-\vartheta(1-\vartheta)(2-\vartheta)/6$, hence

$$|w_{-1}|\le\frac{1}{3}\vartheta(1-\vartheta)\le|\delta|/(3\Delta x),\ \text{and}\ |v(-\Delta x)-P(-\Delta x)|\le\frac{\Delta x^3}{6}\|v'''\|_{\infty,[-\Delta x,0]}$$

because $P'''=0$. □

Uniformity, endpoint cases and nature of the estimate. (a) The constants $\frac{3}{32}$ and $\frac{1}{18}$ are absolute: they hold for every cell index $0\le k\le M-2$, every shift δ (any number of cells) and every mesh size. The only problem-dependent quantities are the norms of v''' and v''''. For $k=0$ we take an extension of Hestenes type, $\bar v(-z)=\sum_{l=1}^{5}c_l\,v(z/l)$ for $0\le z\le\Delta x$, with the c_l determined by $\sum_l c_l(-1/l)^m=1$, $m=0,\dots,4$; it is C^4 across $x=0$ and satisfies $\|\bar v^{(m)}\|_{\infty,[-\Delta x,0]}\le c'_m\|v^{(m)}\|_{\infty,[0,\Delta x]}$ with constants c'_m that do not depend on Δx. (b) Endpoint cases of the implementation (Section 3.1): feet $y<0$ carry the exact payoff and produce no interpolation error; feet at a node ($\vartheta=0$) give $p(y)=v(x_k)$, in agreement with (29); for the interior nodes $1\le j\le M-1$, $\delta\le0$ implies $y\le x_{M-1}$, so that (A2) always holds and no extrapolation occurs; the transferred value at $j=M$ is not used. (c) The estimate concerns one application of the transfer to the smooth function $v=\bar u(\cdot,\tau_n)$, with exact nodal data and the exact Taylor polynomial at the ghost node; in the consistency analysis below u is the solution of the truncated problem, whose distance from the solution of the untruncated problem is bounded by (13). It is a one-step (local) estimate. It does not control how errors already present in U^n are propagated by the transfer (this is the subject of Lemma 3, again for a single step), and it is not a stability or convergence result for the complete nonlinear free-boundary algorithm. (d) The bound was also checked numerically: for three test functions, $\Delta x=10^{-1},\dots,10^{-3}$ and shifts of up to 61 cells, the ratio of the error to the right-hand side of (29) never exceeded 1 and approached 1 as $\Delta x\to0$ (the constant is sharp), the ratio for (30) never exceeded 0.88, and that for the case $k=0$ never exceeded 0.50, for all Δx.

We apply Proposition 1 to $v=\bar u(\cdot,\tau_n)$, a C^4 extension of $u(\cdot,\tau_n)$ to $[-\Delta x,x_{\max}]$, and use $|\delta_n|=|\ln S_f(\tau_{n+1})-\ln S_f(\tau_n)|\le\bar s_n\Delta\tau_n$ with $\bar s_n:=\max_{[\tau_n,\tau_{n+1}]}|s|$ (mean value theorem). Nodes whose foot

Corrected Proof

satisfies $x_j + \delta_n < 0$ carry the exact payoff and contribute no interpolation error. Altogether, in the maximum norm over the interior nodes $j = 1, \dots, M-1$,

$$\max_{1\le j\le M-1} |R_j^n| \le \begin{cases} C_1\Delta\tau_n + C_2\Delta x^2 + \rho_n \bar{s}_n\big(C_3\Delta x^3 + C_4\Delta x^2\,\mathbb{I}_n\big), & \theta = 0 \text{ (EFDM) and } \theta = 1 \text{ (IFDM)}, \\ C_1'\Delta\tau_n^2 + C_2\Delta x^2 + \rho_n \bar{s}_n\big(C_3\Delta x^3 + C_4\Delta x^2\,\mathbb{I}_n\big), & \theta = \tfrac{1}{2} \text{ (CNM)}, \end{cases} \tag{31}$$

where $C_1 = \frac{1}{2}\max_j \|w_j''\|_\infty$, $C_1' = \frac{1}{12}\max_j \|w_j'''\|_\infty$, $C_2 = \frac{\sigma^2}{24}\|u_{xxxx}\|_\infty + \frac{|\mu|}{6}\|u_{xxx}\|_\infty$, $C_3 = \frac{3}{32}\|\bar{u}_{xxxx}\|_\infty$, $C_4 = \frac{1}{18}\|\bar{u}_{xxx}\|_\infty$, all norms being taken over

$$[-\Delta x, x_{\max}] \times [\tau_n, \tau_{n+1}], \text{ and } \rho_n = 1 + (1-\theta)\Delta\tau_n\|A\|_\infty \le 1 + (1-\theta)\Delta\tau_n(2\sigma^2/\Delta x^2 + r),$$

accounts for the fact that the interpolation error e enters R^n both as $e/\Delta\tau_n$ and as $(1-\theta)Ae$. The indicator $\mathbb{I}_n$ equals one only at the node whose foot lies in $[0, \Delta x)$, where the Taylor continuation of Section 3.1 is used, and (for $\theta < 1$) at its two neighbours, and it is zero elsewhere. For the IFDM $\rho_n = 1$; for the EFDM $\rho_n \le 3$ by (33); for the CNM ρ_n may be large, and the interpolation term is then bounded by

$$C\bar{s}_n(\Delta x^3 + \Delta\tau_n\Delta x) \le C\bar{s}_n(\Delta x^2 + \Delta\tau_n^2),$$

except at the three nodes next to the front, where it is $O\big(\bar{s}_n(\Delta x^2 + \Delta\tau_n)\big)$. Hence the linear step of the three schemes is locally consistent of order one (EFDM, IFDM) or two (CNM) in time and two in space, on every time interval $[\tau_n, \tau_{n+1}]$ with $\tau_n \ge \tau_* > 0$, at all interior nodes except, for the CNM, the three nodes next to the front mentioned above. The boundary-update equation (24) has a defect $O(\Delta x^3)$ (see Section 3.3). These statements require u to be smooth on the time interval under consideration, which holds for $\tau \ge \tau_* > 0$. However, near expiry $s(\tau)$ is unbounded and the derivatives of u blow up at $(0,0)$ (Section 2.1), so that the constants $C_1, \dots, C_4$ and $\bar{s}_n$ grow without bound as $\tau_* \to 0$. Estimate (31) is therefore a local statement away from the corner $(x,\tau) = (0,0)$; it does not, by itself, give a global rate of convergence, and a uniform time mesh cannot deliver the orders (31). The graded mesh (14) places $O(\sqrt{N})$ steps in the layer $\tau \le T/N$ and restores second-order temporal convergence of the Crank-Nicolson prices in practice (see Table 8) down to an accuracy floor of about 10^{-5} at $M = 800$ (Section 5.2); the global convergence behaviour is assessed only numerically, against independent references (Section 5.2).

4.2 Stability analysis

If we freeze the variable coefficients $\frac{1}{2}\sigma^2 S^2$ and rS of the Black-Scholes operator, the resulting local conditions do not establish stability of the variable-coefficient scheme. In the variable x, however, the difference operator A in (17) has *constant* coefficients, and the velocity term is taken care of by the transfer Π_n. Hence the von Neumann analysis below is exact for the pure initial value problem, and the matrix analysis that follows is exact for the problem with Dirichlet boundary conditions; no freezing of coefficients is involved.

Throughout, the cell Péclet number $\mathrm{Pe} := \frac{|\mu|\Delta x}{\sigma^2}$, $\mu = r - \frac{\sigma^2}{2}$, is assumed to satisfy $\mathrm{Pe} < 1$. This is a very mild condition. In fact, for the eight data sets of Section 5, $\max|\mu|/\sigma^2 \le 1.26$ and $\Delta x \le 0.03$, therefore $\mathrm{Pe} \le 0.04$.

Corrected Proof

4.2.1 Von Neumann analysis

Substituting the Fourier mode $U_j^n = \xi^n e^{\mathrm{i}j\varphi}$, $\varphi \in [-\pi, \pi]$, into A gives the symbol

$$\widehat{A}(\varphi) = ae^{-\mathrm{i}\varphi} + b + ce^{\mathrm{i}\varphi} = -r - \frac{2\sigma^2}{\Delta x^2}\sin^2\frac{\varphi}{2} + \mathrm{i}\,\frac{\mu}{\Delta x}\sin\varphi,$$

and the amplification factor of the θ-scheme is

$$\xi(\varphi) = \frac{1 + (1-\theta)\Delta\tau\widehat{A}(\varphi)}{1 - \theta\Delta\tau\widehat{A}(\varphi)}. \tag{32}$$

We note that for the fully implicit scheme $\xi = 1/\big(1 + r\Delta\tau + \frac{2\sigma^2\Delta\tau}{\Delta x^2}\sin^2\frac{\varphi}{2} - \mathrm{i}\frac{\mu\Delta\tau}{\Delta x}\sin\varphi\big)$, i.e., all real parts in the denominator are positive.

Theorem 1. *Since* $\mathrm{Re}\,\widehat{A}(\varphi) \le -r < 0$*:* (i) *for* $\theta \in [\frac{1}{2}, 1]$ *(CNM, IFDM),* $|\xi(\varphi)| < 1$ *for all* φ *and all* $\Delta\tau > 0$*;* (ii) *for* $\theta = 0$ *(EFDM), if* $\mathrm{Pe} \le 1$ *and*

$$\Delta\tau\Big(\frac{2\sigma^2}{\Delta x^2} + r\Big) \le 2, \tag{33}$$

then $|\xi(\varphi)| \le 1$ *for all* φ*.*

Proof. (i) Let us write $z = \Delta\tau\widehat{A} = -\alpha + \mathrm{i}\beta$ with $\alpha \ge r\Delta\tau > 0$. Then $|1-\theta z|^2 - |1+(1-\theta)z|^2 = 2\alpha + (2\theta-1)(\alpha^2+\beta^2) > 0$ for $\theta \ge \frac{1}{2}$. (ii) Let $y = \sin^2\frac{\varphi}{2} \in [0,1]$, $\kappa = \sigma^2\Delta\tau/(2\Delta x^2)$, $\nu = \mu\Delta\tau/\Delta x$ and $\rho = r\Delta\tau$. Then $\sin^2\varphi = 4y(1-y)$ and $|\xi|^2 = f(y) := (1-\rho-4\kappa y)^2 + 4\nu^2 y(1-y)$ a quadratic in y with leading coefficient $16\kappa^2 - 4\nu^2 \ge 0$ because $|\nu| \le 2\kappa \iff \mathrm{Pe} \le 1$. Thus f is convex and $\max_{[0,1]} f = \max\{f(0), f(1)\} = \max\{(1-\rho)^2, (1-\rho-4\kappa)^2\}$, which is ≤ 1 if and only if $\rho + 4\kappa \le 2$, i.e., (33). □

Condition (33) follows rigorously from $|\xi| \le 1$. In the variable S it reads $\Delta\tau\,(\sigma^2 S^2/\Delta S^2 + r/2)$ which is less than or approximately equal to 1 with $\Delta S \approx S\Delta x$, and hence the restriction is uniform in S on the logarithmic grid.

4.2.2 Matrix analysis with Dirichlet boundary conditions

The one-step matrices of the three schemes are $G_n(\theta) = (I - \theta\Delta\tau_n A)^{-1}(I + (1-\theta)\Delta\tau_n A)$, so that $F_n = G_n(0)$, $B_n^{-1} = G_n(1)$, and the Crank-Nicolson matrix is $G_n(\frac{1}{2})$.

Lemma 2. *Let* $\mathrm{Pe} < 1$*. Then* $ac > 0$*, and with* $D = \mathrm{diag}\big((c/a)^{j/2}\big)_{j=1}^{M-1}$ *the matrix* DAD^{-1} *is symmetric. The eigenvalues of* A *are real and given by*

$$\lambda_k = -r - \frac{\sigma^2}{\Delta x^2} + \frac{\sigma^2}{\Delta x^2}\sqrt{1-\mathrm{Pe}^2}\cos\frac{k\pi}{M}, \qquad k = 1, \dots, M-1, \tag{34}$$

so that $-r - 2\sigma^2/\Delta x^2 < \lambda_k < -r$*. Moreover, the condition number of* D *satisfies*

$$\kappa(D) = \Big(\frac{1+\mathrm{Pe}}{1-\mathrm{Pe}}\Big)^{(M-2)/2} \le \exp\Big(\frac{|\mu|\,x_{\max}}{\sigma^2(1-\mathrm{Pe})}\Big), \tag{35}$$

a bound independent of Δx*.*

Corrected Proof

Proof. We have

$$(DAD^{-1})_{j,j+1} = c\,d_j/d_{j+1} = \sqrt{ac} = a\,d_{j+1}/d_j = (DAD^{-1})_{j+1,j} \text{ for } d_j = (c/a)^{j/2}.$$

The eigenvalues of the symmetric tridiagonal Toeplitz matrix $\operatorname{tridiag}(\sqrt{ac}, b, \sqrt{ac})$ are $b + 2\sqrt{ac}\cos(k\pi/M)$, and $2\sqrt{ac} = \frac{\sigma^2}{\Delta x^2}\sqrt{1-\mathrm{Pe}^2}$. Finally $c/a = (1+\mathrm{Pe})/(1-\mathrm{Pe})$ (for $\mu > 0$; otherwise its reciprocal), $\ln\frac{1+z}{1-z} \le \frac{2z}{1-z}$ for $0 \le z < 1$, and $(M-2)\Delta x \le x_{\max}$. □

Theorem 2 (ℓ_2-stability)**.** *Let* $\mathrm{Pe} < 1$, $\|\mathbf{v}\|_D := \|D\mathbf{v}\|_2$ *and* $g_\theta(z) = \frac{1+(1-\theta)z}{1-\theta z}$. *Then*

$$\|G_n(\theta)\|_D = \max_k \left|g_\theta(\Delta\tau_n\lambda_k)\right|,$$

and $\|G_n(\theta)\|_D < 1$, *(i) for* $\theta \in [\frac{1}{2}, 1]$ *and every* $\Delta\tau_n > 0$, *(ii) for* $\theta = 0$ *whenever* $\Delta\tau_n(2\sigma^2/\Delta x^2 + r) \le 2$. *Consequently, for any sequence of steps satisfying these conditions,*

$$\left\|G_n(\theta)G_{n-1}(\theta)\cdots G_0(\theta)\right\|_2 \le \kappa(D) \le \exp\left(\frac{|\mu|\,x_{\max}}{\sigma^2(1-\mathrm{Pe})}\right).$$

Proof. We know that $DG_n(\theta)D^{-1}$ is a rational function of the symmetric matrix DAD^{-1}, hence symmetric with eigenvalues $g_\theta(\Delta\tau_n\lambda_k)$. For $z < 0$, $|g_\theta(z)| < 1$ when $\theta \ge \frac{1}{2}$, and $|1+z| \le 1$ iff $z \ge -2$; by Lemma 2, $\Delta\tau_n\lambda_k \ge -\Delta\tau_n(2\sigma^2/\Delta x^2 + r)$. The same matrix D symmetrises every G_n, because A does not depend on n; hence $\|\prod G_n\|_2 \le \kappa(D)\prod\|G_n\|_D \le \kappa(D)$. □

For the State Bank of India data, (35) gives $\kappa(D) \approx e^{\mu x_{\max}/\sigma^2} \approx 2.18$ for all grids (see Table 12). Note that $\max_k |g_\theta(\Delta\tau\lambda_k)|$ is exactly the spectral radius of $G_n(\theta)$. Here the spectral radius is computed from the exact eigenvalues (34) of the matrix with Dirichlet boundary conditions rather than from a Fourier mode.

Theorem 3 (Discrete maximum principle)**.** *Let* $\mathrm{Pe} \le 1$, *so that* $a, c \ge 0$ *and* $b < 0$. (i) *(IFDM) For every* $\Delta\tau > 0$, $I - \Delta\tau A$ *is a strictly diagonally dominant M-matrix,* $(I-\Delta\tau A)^{-1} \ge 0$ *entrywise and* $\|(I - \Delta\tau A)^{-1}\|_\infty \le (1 + r\Delta\tau)^{-1}$. (ii) *(EFDM) If* $\Delta\tau(\sigma^2/\Delta x^2 + r) \le 1$, *then* $I + \Delta\tau A \ge 0$ *and* $\|I + \Delta\tau A\|_\infty = 1 - r\Delta\tau$. (iii) *(CNM) If* $\Delta\tau(\sigma^2/\Delta x^2 + r) \le 2$, *then* $G(\frac{1}{2}) \ge 0$ *and* $\|G(\frac{1}{2})\|_\infty \le \frac{1-r\Delta\tau/2}{1+r\Delta\tau/2}$.

Proof. (i) The off-diagonal entries $-\Delta\tau a$, $-\Delta\tau c$ are non-positive and every row satisfies $1 - \Delta\tau b - \Delta\tau(a+c) = 1 + r\Delta\tau > 0$; the bound follows from the standard estimate $\|\mathscr{M}^{-1}\|_\infty \le 1/\min_i(\mathscr{M}\mathbf{1})_i$ for M-matrices. (ii) All entries of $I + \Delta\tau A$ are non-negative under the stated condition, and each row sum equals $1 + \Delta\tau(a+b+c) = 1 - r\Delta\tau$ (rows next to the boundary have smaller sums). (iii) To obtain this results, we combine (i) with $\Delta\tau/2$ and (ii) with $\Delta\tau/2$. □

Theorem 3 implies that the diffusion steps preserve positivity and satisfy a discrete comparison principle; for the fully implicit scheme this holds without any time-step restriction. It is not true, however, that the Crank-Nicolson scheme is contractive in the maximum norm for large $\Delta\tau/\Delta x^2$ (see Table 12); it is stable in ℓ_2 (Theorem 2).

Lemma 3. *Let the foot of the characteristic be* $x_j + \delta = x_{j-\ell} + \vartheta\Delta x$ *with an integer* $\ell \ge 0$ *and* $\vartheta \in [0, 1)$, *so that the transfer (16) reads* $\widetilde{U}_j = \sum_{k=-1}^{2} w_k(\vartheta)U_{j-\ell+k}$ *with the cubic Lagrange weights* $w_{-1} =$

Corrected Proof

$-\frac{1}{6}\vartheta(\vartheta-1)(\vartheta-2)$, $w_0=\frac{1}{2}(\vartheta+1)(\vartheta-1)(\vartheta-2)$, $w_1=-\frac{1}{2}(\vartheta+1)\vartheta(\vartheta-2)$, $w_2=\frac{1}{6}(\vartheta+1)\vartheta(\vartheta-1)$. *Its Fourier symbol is* $e^{-i\ell\varphi}\pi_\vartheta(\varphi)$, $\pi_\vartheta(\varphi)=\sum_{k=-1}^{2} w_k(\vartheta)e^{ik\varphi}$, *and with* $y=\sin^2\frac{\varphi}{2}$,

$$1-|\pi_\vartheta(\varphi)|^2=\frac{4}{9}\,\vartheta(1-\vartheta)(1+\vartheta)(2-\vartheta)\,y^2\big(3+4\vartheta(1-\vartheta)y\big)\ \geq 0. \tag{36}$$

Hence $|\pi_\vartheta(\varphi)|\leq 1$ *for all* $\vartheta\in[0,1]$, $\varphi\in[-\pi,\pi]$ *and every shift (any* ℓ*), i.e., a single transfer step is von Neumann stable [8], with equality only for* $\varphi=0$ *or* $\vartheta\in\{0,1\}$. *Its maximum norm is* $\sum_k|w_k(\vartheta)|=1+\vartheta(1-\vartheta)\leq\frac{5}{4}$, *hence the transfer is not a contraction in* ℓ_∞.

Proof. Since $\sum_k w_k=1$, $|\pi_\vartheta|^2=\sum_{k,l}w_kw_l\cos((k-l)\varphi)$. Writing $\cos\varphi=1-2y$, $\cos2\varphi=1-8y+8y^2$, $\cos3\varphi=1-18y+48y^2-32y^3$ and collecting powers of y, the coefficient of y is

$$-2\sum_{k,l}w_kw_l(k-l)^2=-4\Big[\sum_k k^2w_k-\Big(\sum_k kw_k\Big)^2\Big]=0,$$

because cubic interpolation reproduces 1, k and k^2 exactly ($\sum_k kw_k=\vartheta$, $\sum_k k^2w_k=\vartheta^2$). The remaining coefficients of y^2 and y^3 factorise as in (36); this elementary but lengthy computation was also checked numerically. All factors in (36) are non-negative for $\vartheta\in[0,1]$, $y\in[0,1]$. The shift by ℓ whole cells only multiplies the symbol by $e^{-i\ell\varphi}$. Finally, for $\vartheta\in[0,1]$ we have

$$w_{-1},w_2\leq 0\leq w_0,w_1 \text{ and } w_{-1}+w_2=-\frac{1}{2}\vartheta(1-\vartheta),$$

hence $\sum_k|w_k|=\sum_k w_k-2(w_{-1}+w_2)=1+\vartheta(1-\vartheta)$. □

Remark 2. *Lemma 3 concerns the transfer as a linear operator on the infinite uniform grid with a fixed shift. Combined with Theorem 1 it shows that, for a* prescribed *sequence of shifts* δ_n, *the symbol of the composite linear step* $U^n\mapsto G_n(\theta)\Pi_nU^n$ *of the pure initial value problem has modulus at most one (for* $\theta\in[\frac{1}{2},1]$, *and for* $\theta=0$ *under (33)), so that this composite step does not amplify any Fourier mode. It does not cover the boundary* $x=0$ *(exact payoff for feet in the exercise region, Taylor continuation), the truncation at* $x_{\max}$, *the Dirichlet setting of Theorem 2 (the transfer is not symmetrised by D), or the dependence of* δ_n *on the solution through (26). Neither Lemma 3 nor Proposition 1 is therefore a stability or convergence result for the complete algorithm.*

Remark 3. *Theorems 1-3 and Lemma 3 establish the stability of the linear steps of the method (the diffusion step and a single application of the transfer), for a given boundary position* S_f^{n+1} *and a given shift, with constants independent of* Δx *and* $\Delta\tau$. *The complete scheme is nonlinear, because* S_f^{n+1} *is defined by (26), and the Lax-Richtmyer equivalence theorem [18] does not apply to it directly; a convergence proof for front-tracking schemes of this type is, to our knowledge, not available in the literature (for the explicit front-fixing scheme, positivity and stability conditions were established in [5], and for the fixed-grid formulation convergence of the discrete LCP is known [16]). We therefore do not claim a stability or convergence theorem for the coupled scheme. Instead, (a) the errors in Section 5 are measured against independent reference solutions rather than by a double-mesh principle, (b) the observed orders are compared with (31), and (c) the discrete complementarity conditions are verified a posteriori (Table 15).*

Corrected Proof

Remark 4. *If the term su_x is discretised directly by central differences with $s^{n+1/2} = \delta_n/\Delta\tau_n$, the coefficient μ in (17) becomes $\mu_n = r - \sigma^2/2 + s^{n+1/2}$ and changes from step to step. Near expiry $|s^{n+1/2}|$ is very large, the cell Péclet number $|\mu_n|\Delta x/\sigma^2$ exceeds one by orders of magnitude, and the M-matrix property of Theorem 3 is lost. For the fully implicit scheme the discrete boundary equation then has a spurious root: the computed exercise boundary is too low and does not converge as the mesh is refined (Table 11). This is the reason for the characteristic treatment of Section 3.1.*

4.3 Summary: what is proved and what is not

For clarity we list the scope of the analysis of this section.

(i) *Linear diffusion step for a prescribed boundary position.* For a given S_f^{n+1} the diffusion step is stable: the von Neumann result of Theorem 1 holds for the constant-coefficient operator (unconditionally for $\theta \in [\frac{1}{2}, 1]$, under the time-step restriction (33) and $\mathrm{Pe} \leq 1$ for the EFDM); the ℓ_2 bound of Theorem 2 holds with Dirichlet boundary conditions for $\mathrm{Pe} < 1$ (unconditionally for $\theta \in [\frac{1}{2}, 1]$, under (33) for the EFDM); the discrete maximum principle of Theorem 3 holds unconditionally only for the IFDM, and for the EFDM and CNM under the stated restrictions on $\Delta\tau(\sigma^2/\Delta x^2 + r)$.

(ii) *Transfer (one-step results).* The interpolation error of one transfer step is bounded with constants $\frac{3}{32}$ and $\frac{1}{18}$ that do not depend on the shift, the cell index or the mesh size (Proposition 1), a single transfer step is von Neumann stable for every shift (Lemma 3, proved analytically), and its maximum norm is at most $\frac{5}{4}$. These are one-step estimates; they enter the local truncation error and do not imply stability or convergence of the coupled scheme. The consistency estimate (31) is local and requires smoothness, i.e., it holds on $\tau \geq \tau_* > 0$ with constants that are unbounded as $\tau_* \to 0$.

(iii) *Coupled problem.* No existence or uniqueness result for the root of the boundary equation (26) and no stability or convergence theorem for the fully coupled nonlinear scheme, in which S_f^{n+1} is determined through (26), is proved. In particular, the unconditional stability of the linear step of the IFDM does not imply unconditional stability of the nonlinear free-boundary solve. The behaviour of the coupled scheme is assessed numerically: by errors against independent references (Section 5.2), by the shift ratios (Section 5.2.1), by numerical scans of F_n, which show a single root for the tested parameter sets but do not prove existence or uniqueness (Section 5.6.1), and by a posteriori checks of the complementarity conditions (Table 15).

5 Numerical results

In this section, we present relevant numerical results justifying theoretical outcomes. All computations use the transformed variable $x = \ln(S/S_f(\tau))$ of Section 2.1 with $x_{\max} = 1.5$ and the graded mesh (14) unless stated otherwise. The market data considered in this paper are obtained from two public sector banks, namely State Bank of India (SBI) and Central Bank of India (CBI), and two private sector banks, namely Axis Bank and Kotak Mahindra Bank (Kotak). For State Bank of India, the three-month and six-month datasets correspond to $K = 800$ and $K = 860$, respectively. For Central Bank of India, the corresponding strikes are $K = 64$ and $K = 68$. Similarly, for Axis Bank, the three-month and six-month datasets are associated with $K = 1250$ and $K = 1200$, while for Kotak Mahindra Bank they correspond

Corrected Proof

Table 2: Sample windows of the eight data sets, number of daily closing prices and historical close-to-close volatility (37)

Bank	window	first trading day	last trading day	closing prices	$\hat{\sigma}_{CC}$	K
SBI	3 months	17-Sep-2024	16-Dec-2024	62	0.2525	800
SBI	6 months	18-June-2024	16-Dec-2024	125	0.2342	860
CBI	3 months	17-Sep-2024	16-Dec-2024	62	0.4274	64
CBI	6 months	18-June-2024	16-Dec-2024	125	0.3455	68
Axis	3 months	17-Sep-2024	16-Dec-2024	62	0.2400	1250
Axis	6 months	18-June-2024	16-Dec-2024	125	0.2230	1200
Kotak	3 months	17-Sep-2024	16-Dec-2024	62	0.2081	1875
Kotak	6 months	18-June-2024	16-Dec-2024	125	0.1923	1735

to $K = 1875$ and $K = 1735$, respectively. The spot prices S_0 in the tables are chosen around the strike and within the range of prices observed in the respective windows.

Nature of the study and data. The strikes, maturities and spot prices define *hypothetical* American put contracts on the four stocks; their values are computed with parameters estimated from historical stock prices (Section 5.1). Exchange-traded single-stock options in India are European-style, so no market prices of American puts are available for comparison, and the study is a model-parameter study, not an empirical validation against traded contracts. The four stocks pay dividends, which are omitted: the contracts are valued as American puts on non-dividend-paying stocks with the estimated volatilities, and the effect of a dividend yield is quantified in Table 5. The model inputs are estimated from these data; the data do not, and are not used to, validate the method against traded American-option prices.

Data source and documentation. The daily prices were obtained from the National Stock Exchange of India (NSE). For each stock (NSE symbols SBIN, CENTRALBK, AXISBANK and KOTAKBANK, series EQ), the security-wise historical data of the equity segment were downloaded as CSV files from the *Historical Data* section of the NSE quote pages (`https://www.nseindia.com`). For every trading day these files contain the open, high, low, previous close (PREV. CLOSE), last traded price, close, volume-weighted average price and 52-week high and low. We use the official closing price (field *close*), not the last traded price, and for the range-based estimators of Table 3 the fields *open*, *high* and *low*. The prices are unadjusted, as published by NSE: they are not adjusted for dividends or other corporate actions. On every trading day of all eight windows the field PREV. CLOSE equals the close of the preceding trading day, i.e., no base-price adjustment for a corporate action occurred in the windows, and the largest absolute daily log-return is 8.1% (CBI). Cash dividends paid within a window are not removed; the corresponding price change enters (37) as an ordinary daily return. All eight series are supplied, unchanged, in the supplementary workbook `Three_and_six_month_data_files.xlsx` (Supplementary file S1), one sheet per bank and window (e.g., sheet `CBI-3`); the volatilities in Table 2 are reproduced from it by the supplied code. Table 2 lists the first and last trading day and the number of closing prices of each window.

5.1 Model inputs: volatility and risk-free rate

Volatility. The volatilities are *historical* volatilities. For each bank and each window (e.g., for Central Bank of India, three months: 62 trading days from 17 September to 16 December 2024, sheet `CBI-3` of Supplementary file S1; all windows in Table 2) let $C_0, \ldots, C_n$ be the daily closing prices (field *close*) and $R_i = \ln(C_i/C_{i-1})$, $i = 1, \ldots, n$, the daily log-returns ($n = 61$ for the three-month and $n = 124$ for the

Corrected Proof

Table 3: Volatility estimates for CBI (three months, sheet `CBI-3` of Supplementary file S1) and the resulting American (CNM, $M = N = 400$) and European put values at $S_0 = 58$ and exercise boundary $S_f(T)$ at the valuation date; $K = 64$, $r = 0.065$, $T = 0.25$. The values are computed with the unrounded estimates (e.g., $\hat{\sigma}_{\mathrm{CC}} = 0.427384$); all other tables use the rounded values, e.g., $\sigma = 0.4274$, which explains the small differences from Table 13 (8.1830, $S_f(T) = 45.3332$).

Estimator	$\hat{\sigma}$	American put	European put	$S_f(T)$
Close-to-close	0.4274	8.1828	8.0051	45.3340
Parkinson [23]	0.3900	7.7836	7.5916	47.0520
Garman-Klass [12]	0.3971	7.8585	7.6695	46.7234
Rogers-Satchell [26]	0.3928	7.8132	7.6224	46.9216
Yang-Zhang [29]	0.4104	8.0006	7.8168	46.1082

six-month windows). The volatility is the annualised sample standard deviation

$$\hat{\sigma}_{\mathrm{CC}} = \sqrt{\frac{252}{n-1}\sum_{i=1}^{n}\left(R_i - \bar{R}\right)^2}, \qquad \bar{R} = \frac{1}{n}\sum_{i=1}^{n} R_i, \tag{37}$$

with 252 trading days per year. This gives $\sigma = 0.2525$ (SBI), 0.4274 (CBI), 0.2400 (Axis) and 0.2081 (Kotak) for the three-month windows, and 0.2342, 0.3455, 0.2230 and 0.1923 for the six-month windows. (The values above are close-to-close estimates; they are reproduced to all digits from Supplementary file S1 by the supplied code, e.g., $\hat{\sigma}_{\mathrm{CC}} = 0.427384$ for CBI, three months.) To assess this choice, in Table 3, we compare (37) with the range-based estimators of Parkinson [23], Garman and Klass [12], Rogers and Satchell [26] and Yang and Zhang [29], which also use the daily open (O_i), high (H_i) and low (L_i) prices, e.g.,

$$\hat{\sigma}^2_{\mathrm{P}} = \frac{252}{4(n+1)\ln 2}\sum_{i=0}^{n}\ln^2\frac{H_i}{L_i}, \qquad \hat{\sigma}^2_{\mathrm{GK}} = \frac{252}{n+1}\sum_{i=0}^{n}\left[\frac{1}{2}\ln^2\frac{H_i}{L_i} - (2\ln 2 - 1)\ln^2\frac{C_i}{O_i}\right],$$

i.e., the Parkinson, Garman-Klass and Rogers-Satchell estimators average over all $n+1$ daily bars, while the Yang-Zhang estimator uses the n days with an overnight return $\ln(O_i/C_{i-1})$. For the CBI data the range-based estimates are 4-9% lower than $\hat{\sigma}_{\mathrm{CC}}$, because they ignore (or, for Yang-Zhang, only partly capture) overnight price changes; the American put value at $S_0 = 58$ (the closing price on 16 December 2024) changes by at most 0.40, i.e., by less than 5%.

We used historical rather than implied volatilities for two reasons. First, our aim is to compare numerical methods on realistic parameter sets, and historical estimates are available in a uniform way for all four stocks. Second, exchange-traded single-stock options in India are European-style, and liquid option quotes over the sample windows were not available to us for all four stocks. Where such quotes exist, an implied volatility could be substituted directly in (7); Table 3 indicates the size of the effect of such a change.

Risk-free rate. Initially, we have tested the performance of our approach for the base lending (home-loan) rates of the banks (8.50% and 8.75%). However, these are lending rates that contain credit and term premia and are not risk-free rates. We therefore used the policy repo rate of the Reserve Bank of India, $r = 6.50\%$, which was unchanged from February 2023 to February 2025 and hence over all sample windows [25]. Table 4 shows the sensitivity of the American put values and exercise boundaries to r, including the rates that we initially used.

A higher rate lowers the put value and raises the exercise boundary (early exercise becomes more attractive because the strike can earn interest earlier). Moving from the lending rates to the repo rate

Corrected Proof

Table 4: Sensitivity to the risk-free rate: American put value (CNM, $M = N = 400$) and, in parentheses, the exercise boundary $S_f(T)$ for the three-month contracts. The last column contains the lending rate used for additional tests.

Bank	S_0	$r = 5.5\%$	$r = 6.5\%$ (base)	$r = 7.5\%$	Put ($S_f(T)$) [rate]
SBI	775	48.2143 (664.238)	47.4032 (670.864)	46.6222 (676.646)	45.8688 (681.777) [8.50 %]
CBI	58	8.2583 (44.6168)	8.1830 (45.3332)	8.1101 (45.9644)	8.0394 (46.5297) [8.50 %]
Axis	1220	67.4285 (1050.262)	66.1947 (1060.257)	65.0060 (1068.972)	63.5790 (1078.501) [8.75 %]
Kotak	1840	84.3778 (1622.927)	82.6041 (1636.455)	80.9011 (1648.215)	78.8649 (1661.034) [8.75 %]

increases the American put values by about 2-5%.

Dividends. The four stocks pay dividends, which are omitted in the contracts valued in this paper. To indicate the size of this simplification, Table 5 gives the three-month values for a continuous dividend yield q. With $q \le r$ the boundary still starts at $S_f(0) = K$, the drift in (15) becomes $\mu = r - q - \sigma^2/2$, the curvature condition of Lemma 1 becomes $u_{xx}(0,\tau) = 2(rK - qS_f)/\sigma^2 - S_f$, and the update (24) becomes

$$S_f^{n+1} = \left(K(1 + r\Delta x^2/\sigma^2) - U_1^{n+1}\right)/\left(1 + \Delta x + \Delta x^2/2 + q\Delta x^2/\sigma^2\right),$$

otherwise the method is unchanged. A yield of 1% (2%) raises the put values by 0.8-2.0% (1.6-4.1%) and lowers the exercise boundary by 0.7-1.2% (1.6-2.5%); the errors with respect to BBSR (with the same yield) are unchanged. Discrete dividends are left for future work (Section 6).

Table 5: Effect of a continuous dividend yield q on the three-month contracts: American put value (CNM, $M = N = 400$), its error with respect to BBSR ($N_b = 20000$, same q) and, in parentheses, the exercise boundary $S_f(T)$

Bank	S_0	$q = 0$	$q = 0.5\%$	$q = 1\%$	$q = 2\%$	max. error
SBI	775	47.4032 (670.864)	47.7700 (668.092)	48.1432 (665.157)	48.9075 (658.724)	3.7e-03
CBI	58	8.1830 (45.3332)	8.2144 (45.0699)	8.2462 (44.7954)	8.3109 (44.2090)	1.5e-04
Axis	1220	66.1947 (1060.257)	66.7566 (1056.037)	67.3276 (1051.567)	68.4987 (1041.742)	6.2e-03
Kotak	1840	82.6041 (1636.455)	83.4215 (1630.619)	84.2537 (1624.415)	85.9645 (1610.700)	1.1e-02

5.2 Error study against independent references

Four kinds of evidence statements (ES) are distinguished in this section and in the rest of the paper. (ES1) *Local consistency*: the truncation error of the linear step for smooth solutions, away from $(x,\tau) = (0,0)$; it is proved (Section 4.1). (ES2) *Grid-difference evidence*: differences between results of the same method on different grids, i.e., errors against a same-grid fine-step solution (Tables 8 and 10) or the refinement of the reference itself (Table 6); it shows that the computed numbers settle, but not what they settle to. (ES3) *Independent-reference comparisons*: errors against the integral-equation solution or BBSR, which share no component with the finite difference schemes (Tables 7, 14, 11, 19, 21 and 18). (ES4) *Global convergence* of the coupled scheme: it is not proved, and the orders observed under (ES3) are numerical observations for the tested parameter sets, not consequences of a theorem. Each table caption states which kind of evidence it provides and how its errors are defined.

Since no closed-form solution is available for the American put, self-referencing (double-mesh) differences, which are evidence of type (ES2), cannot validate a convergence theory. We therefore measure errors against reference solutions computed by methods that are independent of the finite difference schemes:

Corrected Proof

- Exercise boundary and option values (independent reference): the early-exercise-premium representation of Kim [17] and Carr et al. [6],

$$V(S,\tau) = p_E(S,\tau) + rK\int_0^\tau e^{-r(\tau-v)}\,\mathcal{N}\big(-d_-(\tau-v, S/S_f(v))\big)\,dv,\quad d_\pm(\tau,z) = \frac{\ln z + (r \pm \sigma^2/2)\tau}{\sigma\sqrt{\tau}}, \tag{38}$$

where p_E is the Black-Scholes European put and $\mathcal{N}$ the standard normal distribution function, together with the smooth-pasting condition $\partial_S V(S_f(\tau),\tau) = -1$, which gives an integral equation (IE) for S_f. We solve it on the nodes $\tau_i = T(i/n)^2$, interpolating $\ln S_f$ by local cubic polynomials in $\sqrt{\tau}$ and computing the integrals by 8-point Gauss-Legendre quadrature on every subinterval, with the substitution $v = \tau_i - z^2$ on the last one; $S_f(\tau_i)$ is computed by a secant iteration. The option values then follow from (38). This method shares no component with the finite difference schemes (no grid in S, no time stepping of the PDE). Its accuracy is documented in Table 6: with $n = 2000$ the boundary $S_f(T)$ is converged to about 10^{-9} (in n and in the number of Gauss points), and the value-matching condition $V(S_f,\tau) = K - S_f$, which is not imposed, is satisfied to within $6.3\times10^{-11}K$ at all nodes for $n = 2000$ (Table 6). We use $n = 2000$.

- Option values (second reference): the binomial Black-Scholes method with Richardson extrapolation (BBSR) of Broadie and Detemple [4],

$$V_{\mathrm{BBSR}}(N_b) = 2V_{\mathrm{BBS}}^{(N_b)} - V_{\mathrm{BBS}}^{(N_b/2)}, \tag{39}$$

where $V_{\mathrm{BBS}}^{(N)}$ denotes the value of the Cox-Ross-Rubinstein tree [7] with N steps ($\Delta t = T/N$, $u = e^{\sigma\sqrt{\Delta t}}$, $d = 1/u$, $p = (e^{r\Delta t} - d)/(u-d)$) in which the continuation value at the last step before expiry is replaced by the Black-Scholes value. The extrapolation (39) eliminates the term proportional to $1/N$ in the error of the BBS method. We use $N_b = 20000$, i.e., the trees with 20000 and 10000 steps; "BBSR with N_b" always denotes the pair $(N_b, N_b/2)$. For CBI (three months) the maximal differences over the six spot prices are 3.8×10^{-6} between $N_b = 10000$ (trees with 10000 and 5000 steps) and $N_b = 20000$, 1.9×10^{-6} between $N_b = 20000$ and $N_b = 40000$ (trees with 40000 and 20000 steps), and 1.9×10^{-6} between BBSR ($N_b = 20000$) and the integral-equation values. For all 48 cases of Table 13 BBSR and the integral-equation values agree to within 8×10^{-7} relative (3.8×10^{-5} absolute).

- Grid refinement of the front-tracking CNM itself (not an independent reference): with $N = 8M$, the boundaries $S_f(T)$ for $M = 800$, 1600 and 3200 differ from the integral-equation value by -1.8×10^{-5}, -1.6×10^{-6} and $+8.0\times10^{-7}$, respectively (Table 6).

The errors reported are $e_V = \max_i |V(S_0^{(i)},T) - V_{\mathrm{ref}}(S_0^{(i)})|$ over the six spot prices of Table 13 and $e_S = |S_f^N - S_f^{\mathrm{ref}}(T)|$, both with respect to the integral-equation reference, whose uncertainty (less than or approximately equal to 10^{-8}) is far below all reported errors; the observed order is $\log_2(e^{(M)}/e^{(2M)})$. The parameters are those of Central Bank of India (three months: $K = 64$, $r = 0.065$, $T = 0.25$, $\sigma = 0.4274$, the most volatile data set).

In Table 7, we present the results where we refine space and time together: for the EFDM the number of time steps is dictated by Theorem 3(ii), $N = \lceil 2T(\sigma^2/\Delta x^2 + r)/0.9\rceil$ (the largest step of the graded mesh is about $2T/N$), for the IFDM $\Delta\tau \propto \Delta x^2$ ($N = M^2/25$) to balance its first-order temporal error, and for

Corrected Proof

Table 6: Accuracy of the reference solutions. Top: integral-equation (IE) boundary $S_f(T)$ for n nodes and G Gauss points, and maximal value-matching residual $\max_i |V(S_f(\tau_i),\tau_i) - (K - S_f(\tau_i))|/K$ for $n = 2000$, $G = 8$. Bottom: front-tracking CNM boundaries with $N = 8M$ (CBI, three months) and their differences from the IE value

	IE, $G = 8$				IE, $G = 12$	VM residual
data set	$n = 250$	$n = 500$	$n = 1000$	$n = 2000$	$n = 2000$	$/K$
SBI, 3 m	670.860948788	670.860948773	670.860948771	670.860948771	670.860948771	2.9e-11
SBI, 6 m	706.860909879	706.860909855	706.860909852	706.860909852	706.860909852	6.1e-11
CBI, 3 m	45.332378173	45.332378172	45.332378171	45.332378171	45.332378171	2.6e-11
CBI, 6 m	48.904738629	48.904738627	48.904738626	48.904738626	48.904738626	5.8e-11
Axis, 3 m	1060.252168495	1060.252168472	1060.252168469	1060.252168469	1060.252168469	2.9e-11
Axis, 6 m	999.025315016	999.025314982	999.025314978	999.025314978	999.025314978	6.2e-11
Kotak, 3 m	1636.446083583	1636.446083549	1636.446083545	1636.446083545	1636.446083545	3.0e-11
Kotak, 6 m	1494.795963114	1494.795963068	1494.795963063	1494.795963062	1494.795963062	6.3e-11
FT-CNM, CBI 3 m	$M = 800$	$M = 1600$	$M = 3200$	IE ($n = 2000$)		
$S_f(T)$, $N = 8M$	45.33236033	45.33237662	45.33237897	45.33237817		
difference to IE	-1.78×10^{-5}	-1.55×10^{-6}	$+7.95 \times 10^{-7}$	–		

the CNM $\Delta\tau \propto \Delta x$ ($N = 4M$). All three schemes converge. The observed orders of the option values increase towards two (EFDM 1.27-1.82, IFDM 1.93-1.97, CNM 1.85-1.94), and those of the exercise boundary are about two for the EFDM (2.08-2.24) and the IFDM (1.82-2.19), in agreement with (31).

For the CNM the boundary orders on the three finest grids (2.44, 2.99, 2.97) are larger than two and are not measured asymptotic rates. The signed error $S_f^N - S_f^{\mathrm{ref}}(T)$ in Table 7 changes sign between $M = 400$ and $M = 800$, because it is the sum of a negative spatial part and a positive temporal part which almost cancel on the finest grid. With $N = 12800$ steps, where the temporal error is negligible, the spatial parts are -2.70×10^{-3}, -5.82×10^{-4}, -1.22×10^{-4} and -2.41×10^{-5} for $M = 100, \ldots, 800$ (orders 2.21, 2.25, 2.34). The corresponding temporal parts for $N = 4M$ are $+3.34 \times 10^{-4}$, $+1.46 \times 10^{-4}$, $+6.72 \times 10^{-5}$ and $+3.11 \times 10^{-5}$, and at $M = 800$ their sum is only $+7.0 \times 10^{-6}$. On the next finer grid ($M = 1600$, $N = 6400$; not included in the table) the boundary error is -2.1×10^{-6} and the price error is 7.6×10^{-6}. At this level the errors of the CNM are affected by an irregular dependence on N at fixed Δx, which is described below for Table 8, so that no rate is inferred from them. This is not an effect of the reference: all errors in Table 7, including the smallest one (7.0×10^{-6} for the CNM boundary with $M = 800$), exceed the uncertainty of the reference (less than or approximately equal to 10^{-8}) by more than two orders of magnitude.

The run times in Table 7 are medians of three runs, measured as specified in Section 5.6. For $e_V \approx 5 \times 10^{-5}$ the EFDM ($M = 400$) needs 2.6 seconds and the CNM ($M = 800$, $N = 3200$) 1.9 seconds, while the IFDM does not reach this accuracy in the tested range (9.3×10^{-5} in 14.5 seconds for $M = 800$). At equal M the EFDM has the smallest price errors, because its time steps $\Delta\tau \propto \Delta x^2$ make its temporal error small; however, its cost grows like M^3, compared with M^2 for the CNM with $N \propto M$ (13.4 versus 1.9 seconds at $M = 800$). The coupling $N = 4M$ is conservative for the CNM: at $M = 400$, the CNM with $N = 400$ steps has $e_V = 1.7 \times 10^{-4}$ in 0.18 seconds (Table 18), compared with 2.0×10^{-4} in 0.77 seconds with $N = 1600$. Run times at matched accuracy for all five methods are compared in Section 5.7. The same data are shown in Figure 1.

In Table 8, we isolate the temporal error: $M = 800$ is fixed and the errors are measured against the CNM solution with $N = 12800$ on the same spatial grid. For the two blocks on the graded mesh the reference is the graded-mesh solution; for the uniform-mesh block it is the uniform-mesh solution with $N = 12800$ (the statement in the previous version that the same reference was used for all three blocks was incorrect). The IFDM prices are of first order in time (orders 0.98-1.00). The CNM on the graded

Corrected Proof

Table 7: Joint refinement in space and time (CBI, three months, $K = 64$, $r = 0.065$, $T = 0.25$, $\sigma = 0.4274$, $x_{\max} = 1.5$, graded mesh; type (ES3)): errors $e_V = \max_j |V(S_0^{(j)}) - V_{\mathrm{IE}}(S_0^{(j)})|$ over the six spot prices of Table 13 with respect to the integral-equation reference (option values and exercise boundary $S_f(T)$), observed orders and run times (seconds, median of three runs). Errors recomputed against the integral-equation reference; the boundary error is given with its sign, $e_S = S_f^N - S_f^{\mathrm{ref}}(T)$, and the order is $\log_2 |e_S^{(M)}/e_S^{(2M)}|$

Scheme	M	N	e_V	order	e_S (signed)	order	time (s)
EFDM	50	113	1.36e-03	-	−1.10e-02	-	0.05
	100	452	5.65e-04	1.27	−2.61e-03	2.08	0.12
	200	1805	1.89e-04	1.58	−5.71e-04	2.19	0.39
	400	7217	5.71e-05	1.73	−1.21e-04	2.24	2.57
	800	28867	1.62e-05	1.82	−2.57e-05	2.24	13.43
IFDM	50	100	2.08e-02	-	−7.90e-03	-	0.04
	100	400	5.45e-03	1.93	−2.23e-03	1.82	0.12
	200	1600	1.42e-03	1.94	−5.28e-04	2.08	0.44
	400	6400	3.65e-04	1.96	−1.18e-04	2.17	3.12
	800	25600	9.32e-05	1.97	−2.58e-05	2.19	14.50
CNM	50	200	9.94e-03	-	−1.09e-02	-	0.06
	100	400	2.76e-03	1.85	−2.37e-03	2.20	0.10
	200	800	7.43e-04	1.89	−4.36e-04	2.44	0.20
	400	1600	1.96e-04	1.92	−5.48e-05	2.99†	0.77
	800	3200	5.10e-05	1.94	+7.00e-06	2.97†	1.87

†Spatial and temporal error parts of opposite sign nearly cancel; not an asymptotic rate (see the text).

mesh is of second order for $S_f(T)$ from $N = 100$ on (orders 1.99, 2.00, 1.99), and for the option values up to $N = 400$, with orders 2.08, 2.32, 1.54 and 1.99, i.e., 1.98 on average between $N = 25$ and $N = 400$.

On the finest levels the errors approach an accuracy floor of this same-grid comparison, and the orders marked by an asterisk in Table 8 are not measured rates. The floor is not caused by the reference, whose own temporal error is far smaller. It is caused by an irregular, non-monotone dependence of the errors on N at fixed Δx. For the CNM prices the error is 3.3×10^{-6} at $N = 800$, but 1.6×10^{-5} at $N = 1600$ and 4.7×10^{-7} at $N = 3200$ (not included in the table). The IFDM boundary errors are -6.1×10^{-5}, -8.0×10^{-6}, -3.7×10^{-5} and $+4.7 \times 10^{-7}$ for $N = 400$, 800, 1600, 3200, so that the IFDM boundary orders 1.10 and 2.94 are not rates either. This contribution decreases with Δx: for $M = 1600$ (errors against $N = 12800$ on that grid) the CNM price errors for $400 \le N \le 3200$ are at most 4.5×10^{-6}. We attribute it to the terms of (31) at the nodes next to the front (the start-up step of Section 5.2.1 and the Taylor continuation of the transfer). These terms depend on the position of the feet of the characteristics relative to the grid, and hence on N, and therefore do not cancel in a comparison on the same spatial grid. Consequently, at $M = 800$ the temporal convergence of the CNM prices is resolved down to errors of about 10^{-5}; the orders 1.54 ($N = 200$) and 0.32 ($N = 800$) are affected by this contribution.

On a uniform mesh, measured against the uniform-mesh solution with $N = 12800$, the CNM option values converge only at a rate of about one (1.01-1.23 for $N \ge 200$). This reference is itself less accurate than the graded one: it differs from it by 1.9×10^{-5} in the prices and by -4.6×10^{-5} in $S_f(T)$, i.e., 12800 uniform steps give a larger price error than 400 graded steps (4.1×10^{-6}). This is the effect of the singular behaviour of $S_f(\tau)$ near expiry as discussed in Section 5.10.

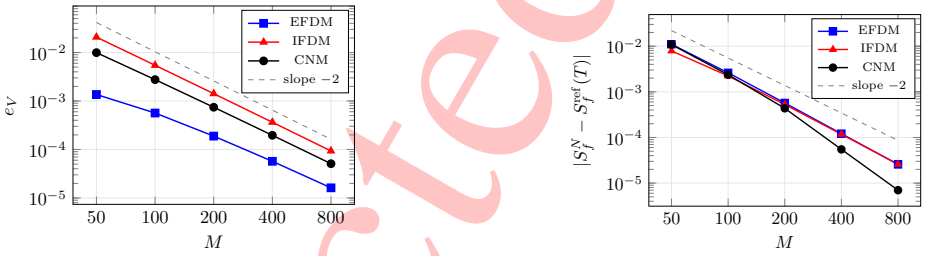
5.2.1 Size of the shifts along the characteristics

In Table 9, we present the shift-to-cell ratios $|\delta_n|/\Delta x$ for the grids of Tables 7 and 8. Two effects are clearly visible:

Corrected Proof

Table 8: Temporal refinement at fixed $M = 800$ (CBI, three months; grid-difference evidence, type (ES2)); errors (e_V: maximum over the six spot prices; e_S: absolute boundary difference) with respect to the same-M solution with $N = 12800$, CNM on the graded mesh (first two blocks) and CNM on the uniform mesh (last block). The last block (uniform mesh) illustrates the effect of the non-smoothness near expiry. *Floor-limited, not a measured rate (irregular dependence on N at fixed Δx, see the text).

Scheme	N	e_V	order	e_S	order
IFDM (graded)	25	4.12e-02	-	4.07e-03	-
	50	2.09e-02	0.98	1.27e-03	1.68
	100	1.05e-02	0.99	4.14e-04	1.62
	200	5.27e-03	1.00	1.30e-04	1.67
	400	2.63e-03	1.00	6.10e-05	1.10
	800	1.32e-03	0.99	7.97e-06	2.94
CNM (graded)	25	9.89e-04	-	1.94e-01	-
	50	2.35e-04	2.08	8.60e-02	1.17
	100	4.70e-05	2.32	3.23e-02	1.41
	200	1.62e-05	1.54	8.12e-03	1.99
	400	4.06e-06	1.99	2.04e-03	2.00
	800	3.26e-06	0.32*	5.11e-04	1.99
CNM (uniform)	25	1.09e-03	-	9.14e-02	-
	50	7.27e-04	0.58	3.43e-02	1.41
	100	2.53e-04	1.52	8.88e-03	1.95
	200	1.10e-04	1.20	2.35e-03	1.92
	400	5.46e-05	1.01	6.65e-04	1.82
	800	2.33e-05	1.23	1.93e-04	1.78



(a) Option values. **(b)** Exercise boundary $S_f(T)$.

Figure 1: Errors under joint refinement (Table 7), CBI, three months ; references: integral-equation solution

(a) *Start-up step.* For all grids of Table 7 the largest ratio occurs at the first step and is almost exactly one, whatever $\Delta\tau_1$; after the first step the ratios are at most 0.17. The reason is the discrete start-up: since $u(x,0) = 0$ for $x > 0$, the value U_1^1 after the first step is very small, and (24) gives

$$\ln(K/S_f^1) = \ln(1+\Delta x+\Delta x^2/2) - \ln(1+r\Delta x^2/\sigma^2) + O(U_1^1) = \Delta x(1 - r\Delta x/\sigma^2) + O(\Delta x^3),$$

i.e., the discrete boundary moves by one cell in the first step. The observed values agree with $1 - r\Delta x/\sigma^2$ (third column of Table 9) to within 0.005. For these grids the exact boundary moves by much less than one cell in the first step (e.g., $\sigma\sqrt{\tau_1|\ln\tau_1|}/\Delta x \approx 0.15$ for the CNM with $M = 800$, $N = 3200$), so in the layer $\sigma\sqrt{\tau|\ln\tau|}$ which is less than or approximately equal to Δx the discrete boundary cannot follow the exact one and carries an error of order Δx; this is the discrete counterpart of the singular behaviour near expiry. The layer is very short (τ which is less than or approximately equal to $\Delta x^2/(\sigma^2|\ln\Delta x^2|)$), and the observed global orders in Table 7 are not affected.

(b) *Multi-cell shifts.* For coarse time meshes the exact boundary moves by several cells in the first steps; then $|\delta_n|$ exceeds Δx at many steps, up to 17.6 cells for the IFDM with $N = 25$ on the graded mesh

Corrected Proof

Table 9: Shift-to-cell ratios $|\delta_n|/\Delta x$ (CBI, three months). Top: grids of Table 7, ratio at the first step / maximum over $n \geq 2$; the column $1 - r\Delta x/\sigma^2$ is the predicted start-up ratio. Bottom: grids of Table 8 ($M = 800$), maximal ratio (attained at the first step) / number of steps with $|\delta_n| > \Delta x$

M	$1 - r\Delta x/\sigma^2$	EFDM	IFDM	CNM
50	0.9893	0.987 / 0.145	0.988 / 0.168	0.985 / 0.083
100	0.9947	0.993 / 0.085	0.993 / 0.099	0.993 / 0.098
200	0.9973	0.996 / 0.049	0.996 / 0.056	0.997 / 0.111
400	0.9987	0.998 / 0.027	0.998 / 0.031	0.999 / 0.124
800	0.9993	0.999 / 0.015	0.999 / 0.017	1.000 / 0.136
N		IFDM (graded)	CNM (graded)	CNM (uniform)
25		17.62 / 25	13.55 / 25	48.02 / 25
50		9.98 / 50	7.82 / 50	36.82 / 50
100		5.77 / 100	4.73 / 100	28.09 / 54
200		3.58 / 58	2.97 / 60	21.36 / 40
400		2.45 / 2	2.05 / 3	16.19 / 27
800		1.92 / 1	1.91 / 1	12.28 / 18

and 48 cells on the uniform mesh (lower part of Table 9). Under the joint refinement with $N \propto M$ the exact first-step shift relative to Δx grows like $\sqrt{\ln N}$, so a one-cell condition cannot be assumed uniformly. This is why the interpolation error is estimated for arbitrary shifts (Proposition 1) and the transfer is shown to be stable for every shift (Lemma 3). For the computations of Tables 13-15 ($M = N = 400$) the first-step ratio lies between 1.00 and 1.82 and all later ratios are at most 0.45.

Finally, the transferred value at x_M that is overwritten by the truncation condition (Section 3.1) never exceeded $10^{-9}K$ in any of the computations of this paper.

5.3 Post-step projection versus discrete complementarity

To address the effect of the projection $V \leftarrow \max(V, K - S)$, in Table 10, we compare for the fixed-grid formulation of Section 3.4 ($M = 1600$, $S_{\max} = 4K$, uniform time steps), the exact solution of the discrete LCP (27) by the Brennan-Schwartz algorithm with the projection. The errors are measured against the same-grid solution with $N = 12800$ (Brennan-Schwartz CNM with Rannacher start), so that only temporal errors are compared. For the fully implicit scheme the projection increases the error by about 25% without changing the (first) order. For the Crank-Nicolson scheme the difference is substantial: with the projection the temporal errors are 8 to 16 times larger than with the exact LCP solution and decay only at first order, i.e., the projection destroys the higher temporal accuracy of the CNM. With the exact LCP solution, the observed order is about 1.3; it is limited by the singular behaviour of the exercise boundary near expiry on a uniform time mesh (see the uniform-mesh block of Table 8). The Rannacher start increases the error constant by a factor of 2-4 (it replaces the first two steps by first-order steps) but does not change the order. This further confirms that the projection is not free of discretization error, and it explains why the double-mesh orders obtained with the projection, could not validate the convergence theory.

5.4 Eulerian versus characteristic treatment of the velocity term

Table 11 supports Remark 4 (SBI, three months; error e_V with respect to BBSR). With the Eulerian discretisation of su_x the EFDM and CNM converge, but the IFDM produces a boundary that is about 1% too low, with price errors of several units which decrease only slowly as the mesh is refined. The characteristic treatment gives convergent results for all three schemes.

Corrected Proof

Table 10: Fixed-grid formulation (CBI, three months, $M = 1600$, $S_{\max} = 4K$, uniform time steps): maximal temporal error of the option values at the six spot prices with respect to the same-grid solution with $N = 12800$ (Brennan-Schwartz CNM with Rannacher start; grid-difference evidence, type (ES2)) for the discrete LCP solved exactly (Brennan-Schwartz) and for the post-step projection. The first two Crank-Nicolson steps are replaced by four implicit half steps. Last column: observed order (least-squares slope over $N = 100, \ldots, 800$)

Method	$N = 25$	50	100	200	400	800	order
IFDM + LCP (Brennan-Schwartz)	3.53e-02	1.83e-02	9.47e-03	4.87e-03	2.49e-03	1.26e-03	0.97
IFDM + projection	4.23e-02	2.23e-02	1.16e-02	6.02e-03	3.09e-03	1.58e-03	0.96
CNM + LCP (Brennan-Schwartz)	1.06e-03	5.33e-04	2.40e-04	1.05e-04	4.43e-05	1.78e-05	1.25
CNM + LCP + Rannacher start	3.98e-03	1.57e-03	6.27e-04	2.54e-04	1.02e-04	4.09e-05	1.31
CNM + projection	9.68e-03	4.36e-03	2.28e-03	1.15e-03	5.80e-04	2.91e-04	0.99
CNM + projection + Rannacher	1.10e-02	4.76e-03	2.41e-03	1.20e-03	5.99e-04	2.99e-04	1.01

Table 11: Eulerian and characteristic ("lagrangian") treatment of the velocity term $s(\tau)u_x$ (SBI, three months, $K = 800$, $\sigma = 0.2525$, $r = 0.065$, $T = 0.25$, graded mesh; $S_f^{\mathrm{ref}}(T) = 670.861$ from the integral equation). $S_f^N \approx S_f(T)$; e_V is the maximal absolute error over the six spot prices of Table 13 with respect to BBSR (type (ES3)).

θ	velocity term	M	N	S_f^N	e_V
0.0	eulerian	100	158	671.0778	1.73e-01
0.0	eulerian	200	630	670.9215	4.54e-02
0.0	eulerian	400	2519	670.8766	1.15e-02
0.0	lagrangian	100	158	670.7820	4.67e-03
0.0	lagrangian	200	630	670.8432	2.18e-03
0.0	lagrangian	400	2519	670.8571	7.88e-04
1.0	eulerian	100	400	648.7639	1.15e+01
1.0	eulerian	200	400	657.5934	6.63e+00
1.0	eulerian	400	400	663.2659	3.65e+00
1.0	lagrangian	100	400	670.8626	7.33e-02
1.0	lagrangian	200	400	670.8823	3.46e-02
1.0	lagrangian	400	400	670.8844	2.39e-02
0.5	eulerian	100	400	670.5164	1.67e-01
0.5	eulerian	200	400	670.7685	4.40e-02
0.5	eulerian	400	400	670.8369	1.13e-02
0.5	lagrangian	100	400	670.8370	5.31e-02
0.5	lagrangian	200	400	670.8595	1.45e-02
0.5	lagrangian	400	400	670.8644	3.89e-03

5.5 Spectral radii

The spectral radii of the one-step matrices $G(\theta)$ of Section 4 are presented in Table 12 for the State Bank of India parameters ($K = 800$, $r = 0.065$, $T = 0.25$, $\sigma = 0.2525$) with $N = 100$ uniform steps ($\Delta\tau = 2.5 \times 10^{-3}$), together with their maximum norms. They are computed from the exact eigenvalues (34) and agree with the eigenvalues of the assembled matrices. In accordance with Theorem 2, the explicit scheme is stable as long as $\Delta\tau \le 2/(2\sigma^2/\Delta x^2 + r)$, i.e., for $M \le 80$ ($\Delta\tau_{\max} = 5.5 \times 10^{-3}$ for $M = 80$ but 1.4×10^{-3} for $M = 160$); for finer grids its spectral radius exceeds one and grows like Δx^{-2}. The IFDM and CNM are stable for all M, with spectral radius $1 - \Delta\tau(r + \sigma^2(1 - \cos(\pi/M))/\Delta x^2) \approx 0.9995$ determined by the smoothest mode. The maximum norm of the CNM matrix exceeds one when $\Delta\tau(\sigma^2/\Delta x^2 + r) > 2$, in agreement with Theorem 3(iii); this does not contradict its ℓ_2-stability.

5.6 American put values for the four banks

In Table 13 (page 29) we present the simulation results for three-month and six-month American put options on non-dividend-paying stocks using five different approaches: the binomial method with Richardson extrapolation (BBSR, $N_b = 20000$), which serves as reference [4, 7], the Longstaff and Schwartz

Corrected Proof

Table 12: Spectral radii $\rho(G)$ and maximum norms $\|G\|_\infty$ of the one-step matrices of the EFDM, IFDM and CNM (SBI, $N = 100$, $\Delta\tau = 2.5 \times 10^{-3}$). Condition number of the symmetriser: $\kappa(D) \in [2.02, 2.18]$

M	Δx	ρ: EFDM	IFDM	CNM	$\|G\|_\infty$: EFDM	IFDM	CNM
20	7.50e-02	0.9995	0.9995	0.9995	0.9998	0.9998	0.9998
40	3.75e-02	0.9995	0.9995	0.9995	0.9998	0.9998	0.9998
80	1.87e-02	0.9995	0.9995	0.9995	0.9998	0.9998	0.9998
160	9.37e-03	2.6268	0.9995	0.9995	2.6272	0.9998	0.9998
320	4.69e-03	13.5079	0.9995	0.9995	13.5083	0.9998	1.6076
640	2.34e-03	57.0321	0.9995	0.9995	57.0325	0.9998	2.2698
1280	1.17e-03	231.1292	0.9995	0.9995	231.1296	0.9998	2.6302

method [19] (denoted as LSM), the Explicit Finite Difference Method (EFDM) (21), the Implicit Finite Difference Method (IFDM) (22), and the Crank-Nicolson Method (CNM) (23). The finite difference results use $M = 400$; the IFDM and CNM use $N = 400$ time steps, and the EFDM uses the number of steps required by Theorem 3(ii)$N = \lceil 2T(\sigma^2/\Delta x^2 + r)/0.9 \rceil$ (between 1711 and 9432). The LSM uses one exercise date per trading day (63 or 126 dates) and the basis $\{1, L_0, L_1, L_2\}$ of weighted Laguerre polynomials in $X = S/K$, $L_0 = e^{-X/2}$, $L_1 = e^{-X/2}(1-X)$, $L_2 = e^{-X/2}(1-2X+X^2/2)$ [19]. We use the out-of-sample (two-pass) version of the method. In the first pass the regression coefficients at every exercise date are estimated by least squares on the in-the-money paths from 10^5 simulated paths; in the second pass the resulting exercise rule is applied to 10^5 independent paths, and the reported value is the mean discounted cash flow of the second pass (exercise at $t = 0$ is allowed). In each pass the 10^5 paths consist of 5×10^4 antithetic pairs $(Z, -Z)$ of exact log-normal time steps, and the standard error given in parentheses is the sample standard deviation of the 5×10^4 pair averages divided by $\sqrt{5 \times 10^4}$. The random numbers are standard normal variates from the Mersenne-twister generator of MATLAB, initialised by `rng(seed,'twister')` with seed $= 1000i + 10j + 1$ (first pass) and $1000i + 10j + 2$ (second pass) for data set $i = 1, \ldots, 8$ (in the order of Table 13) and spot price $j = 1, \ldots, 6$; the normal variates of each pass are generated as one $5 \times 10^4 \times n_d$ array (n_d exercise dates), whose negative supplies the antithetic paths. Since the second-pass estimator is an unbiased estimate of the value of a feasible exercise rule for the Bermudan option, which is worth less than the American option, the LSM values are biased low. Its errors are one to two orders of magnitude larger than those of the finite difference methods (Table 14). Each value in Table 13 is a single run. To quantify the bias and the run-to-run variation, every contract was also priced in 20 independent replications, replication $q = 1, \ldots, 20$ using the seeds $10^5 q + 1000i + 10j + 1$ and $10^5 q + 1000i + 10j + 2$ (Table 16).

Computing environment and run times. The computations presented are performed using MATLAB R2023b on a Lenovo machine (having 16GB RAM running 64-bit operating system) with 12th Gen Intel(R) Core(TM) i7-1260P (2.10 GHz) processor. All run times are elapsed (wall-clock) times in seconds. For each method we specify below what one timed run contains, how often it is repeated, and which summary statistic is reported. All run times are elapsed (wall-clock) times in seconds, measured with `tic`/`toc`. One timed run contains: (i) for the finite difference methods, the complete computation for one data set, i.e., the setup of the grid and matrices, the complete time stepping including all evaluations of F_n and the root search (Sg 1) - (Sg 3), and the evaluation of the six prices; (ii) for BBSR, both trees (N_b and $N_b/2$ steps) for all six spot prices; (iii) for the LSM, both passes, including the generation of the paths and the regressions, for all six spot prices. Nothing is excluded as preprocessing. Each timed run is repeated three times with identical input, and the median of the three times is reported (for the LSM the repetitions reproduce the same paths, which does not affect the timing). Reference computations

Corrected Proof

(integral equation, and BBSR when used as reference) are never included. Run times are reported only together with the corresponding errors: under joint refinement (Table 7) and in the accuracy-matched comparison of Section 5.7. Tables 14 and 19 report no run times, because their methods operate at very different accuracies (e.g., BBSR with $N_b = 20000$ is accurate to about 10^{-6}, the IFDM with $M = N = 400$ only to 10^{-3}-10^{-2}); for them the number of evaluations of F_n is a machine-independent measure of cost. The statements on relative efficiency refer to this implementation and to the parameter sets of the tables.

The CNM errors are between 1.5×10^{-4} (CBI) and 10^{-2} (Kotak, $K = 1875$), i.e., below $6 \times 10^{-6} K$ in all cases, obtained together with the complete price curve and the exercise boundary in less than one second (Table 18). The IFDM is limited by its first-order temporal error ($N = 400$), and the EFDM is more accurate at $M = 400$, because the time-step restriction forces 1711-9432 steps (Table 14); run times at matched accuracy are compared in Section 5.7. The exercise boundaries computed by the three schemes agree to within 0.01% of K.

Replications of the LSM. Table 16 summarises the 20 independent replications of every LSM value (seeds given in Section 5.6; the contract with immediate exercise, CBI six months, $S_0 = 45$, is excluded). For all eight data sets the mean over the replications lies below the integral-equation value: the average bias is between -0.6 and -1.1 single-run standard errors, and 75-87% of the runs lie below the reference. This is the expected low bias of the two-pass estimator, which values a Bermudan option (one exercise date per trading day) with a suboptimal exercise rule. The standard deviation over the replications agrees with the mean reported standard error to within 10%, so that the standard errors in Table 13 are realistic. The LSM errors in Table 14 are therefore dominated by the statistical error, with a systematic low bias of comparable size.

A posteriori verification of the discrete complementarity conditions. In the front-tracking formulation the complementarity conditions (5) are built into the problem: the exercise region $S \le S_f$ carries the payoff exactly, and in the continuation region $S > S_f$ the discrete equation holds with equality. What has to be checked is that the computed solution satisfies the inequality constraints and the qualitative properties of the American put. In Table 15, we list for the CNM solution at $t = 0$ on its grid $S_j = S_f^N e^{x_j}$, the minimum of $U_j - \max(K - S_j, 0)$, the range of the discrete delta $\Delta_j = (U_{j+1} - U_j)/(S_{j+1} - S_j)$ and the minimum of the discrete gamma. In all eight cases $U \ge g$ (with equality only at the free boundary), $-1 \le \Delta \le 0$ and $\Gamma \ge 0$ up to rounding errors, i.e., the computed values are monotone, convex and above the payoff, and the smooth-pasting condition $\Delta \to -1$ at S_f is reproduced.

5.6.1 Numerical check of the root search and of the root of the boundary equation

Failures and statistics of the root search. Every front-tracking computation of this paper was repeated with the root-search statistics recorded at every step: 199 computations with 359 188 time steps and 2 263 550 evaluations of F_n (6.3 per step). No failure of type 1, 2 or 3 (Section 3.3) occurred: $F_n(S_f^n) > 0$ at every step, a sign change was always found, and Brent's method always met the stopping rule. At most 6 bracket expansions were needed (in 83 computations some expansion occurred, always in the first steps), the lower end of the bracket never fell below $0.88\,S_f^n$, Brent's method needed at most 24 iterations (limit 100), and the residual at the accepted root never exceeded $|F_n| = 1.2 \times 10^{-13} K$ (with the tolerance $10^{-6} K$ of Table 19: $1.5 \times 10^{-7} K$).

Number of roots. We have no general existence or uniqueness result for the root of (26) in $(0, S_f^n]$ (Section 4.3), and therefore checked the number of sign changes numerically for the parameter sets of this paper. For the CNM with $M = N = 400$ and all eight data sets, F_n was tabulated at every one of

Corrected Proof

Table 13: Comparative American put option values from five numerical methods for four Indian banks ($r = 0.065$; K, T and σ as in Table 2). BBSR ((39), $N_b = 20000$) is the reference; LSM standard errors in parentheses (two-pass LSM, 10^5 paths per pass, one exercise date per trading day; full specification in the text; "–": immediate exercise is optimal). Finite difference methods: $M = 400$, $x_{\max} = 1.5$, graded mesh, $N = 400$ (IFDM, CNM) and N of Table 14 (EFDM)

Bank	Maturity	S_0	BBSR	LSM (s.e.)	EFDM	IFDM	CNM
SBI	3 months	740	69.5477	69.5170 (0.08339)	69.5471	69.5322	69.5450
		760	56.2096	56.1308 (0.06796)	56.2090	56.1896	56.2063
		775	47.4069	47.2815 (0.06398)	47.4062	47.3844	47.4032
		785	42.1019	41.9760 (0.07120)	42.1013	42.0785	42.0981
		800	34.9651	34.9022 (0.07989)	34.9644	34.9412	34.9612
		820	26.9032	26.8534 (0.08891)	26.9024	26.8806	26.8994
	6 months	805	74.2825	74.1767 (0.09362)	74.2821	74.2583	74.2807
		820	65.4988	65.3187 (0.08740)	65.4984	65.4721	65.4969
		835	57.5158	57.4734 (0.08903)	57.5154	57.4873	57.5138
		855	48.0559	47.8921 (0.10332)	48.0555	48.0264	48.0539
		870	41.7976	41.6423 (0.10299)	41.7971	41.7682	41.7955
		885	36.2082	36.1427 (0.11185)	36.2077	36.1796	36.2061
CBI	3 months	50	14.2629	14.2540 (0.01360)	14.2628	14.2624	14.2628
		55	10.2232	10.2203 (0.01170)	10.2231	10.2216	10.2231
		58	8.1832	8.16501 (0.00924)	8.1831	8.1809	8.1830
		62	5.9255	5.90934 (0.00858)	5.9254	5.9227	5.9253
		65	4.5650	4.55271 (0.01053)	4.5649	4.5622	4.5648
		70	2.8591	2.87009 (0.01152)	2.8591	2.8569	2.8590
	6 months	45	23.0000	23.0000 (–)	23.0000	23.0000	23.0000
		55	13.5825	13.5640 (0.01514)	13.5824	13.5812	13.5824
		60	9.9405	9.94818 (0.01196)	9.9405	9.9380	9.9404
		70	4.8936	4.87881 (0.01234)	4.8936	4.8902	4.8935
		75	3.3068	3.27850 (0.01305)	3.3068	3.3040	3.3067
		85	1.4203	1.40263 (0.01027)	1.4203	1.4194	1.4202
Axis	3 months	1175	93.2269	93.1327 (0.11269)	93.2259	93.2000	93.2220
		1200	77.4414	77.4465 (0.09796)	77.4404	77.4095	77.4358
		1220	66.2008	65.9251 (0.09934)	66.1998	66.1662	66.1947
		1244	54.2987	54.2966 (0.11360)	54.2976	54.2627	54.2924
		1260	47.2891	47.2961 (0.12319)	47.2880	47.2534	47.2828
		1285	37.7334	37.9017 (0.12888)	37.7322	37.6999	37.7273
	6 months	1130	96.2910	96.1306 (0.12357)	96.2904	96.2576	96.2878
		1160	79.3505	79.0667 (0.11644)	79.3500	79.3126	79.3470
		1175	71.7763	71.5896 (0.11975)	71.7757	71.7371	71.7727
		1205	58.3115	58.3395 (0.13877)	58.3108	58.2714	58.3078
		1220	52.3728	52.1534 (0.14514)	52.3722	52.3332	52.3691
		1250	41.9547	41.8903 (0.14951)	41.9539	41.9177	41.9511
Kotak	3 months	1800	105.419	105.244 (0.13141)	105.417	105.377	105.409
		1820	93.5373	93.3224 (0.12720)	93.5358	93.4921	93.5275
		1840	82.6144	82.3251 (0.13435)	82.6128	82.5668	82.6041
		1860	72.6285	72.3248 (0.14514)	72.6269	72.5796	72.6179
		1880	63.5509	63.2131 (0.15698)	63.5492	63.5019	63.5402
		1900	55.3462	55.4163 (0.16437)	55.3443	55.2982	55.3355
	6 months	1640	122.641	122.493 (0.16188)	122.640	122.600	122.636
		1680	99.3573	99.4147 (0.14597)	99.3564	99.3095	99.3507
		1700	89.0479	88.7828 (0.15265)	89.0470	88.9979	89.0410
		1740	70.9143	70.8118 (0.17275)	70.9133	70.8627	70.9071
		1760	63.0114	62.6080 (0.17645)	63.0104	62.9605	63.0043
		1800	49.3253	49.2879 (0.18277)	49.3240	49.2779	49.3184

the 3200 time steps at 400 points of $[10^{-3}S_f^n, S_f^n)$, distributed logarithmically in the relative distance $1 - S/S_f^n \in [10^{-8}, 0.999]$, so that the neighbourhood of the root (whose relative distance from S_f^n lies between 7.8×10^{-5} and 6.5×10^{-3}) is resolved; consecutive points differ by 5% in this distance. At

Computational Proof

Table 14: Maximal absolute errors $e_V = \max_j |V(S_0^{(j)}) - V_{\mathrm{BBSR}}(S_0^{(j)})|$ over the six spot prices of Table 13 with respect to BBSR (39), $N_b = 20000$ (evidence of type (ES3)), finite difference methods with $M = 400$ and $N = 400$ (IFDM, CNM) or N as listed (EFDM), and exercise boundary $S_f(T)$ at the valuation date (CNM). Run times at matched accuracy are given in Table 18.

		max. error e_V					
Bank	T (m)	LSM	EFDM	IFDM	CNM	$S_f(T)$	N (EFDM)
SBI	3	1.26e-01	7.88e-04	2.39e-02	3.89e-03	670.8644	2519
SBI	6	1.80e-01	5.18e-04	2.96e-02	2.11e-03	706.8651	4334
CBI	3	1.81e-02	5.65e-05	2.82e-03	1.69e-04	45.3332	7217
CBI	6	2.83e-02	5.24e-05	3.38e-03	1.45e-04	48.9055	9432
Axis	3	2.76e-01	1.29e-03	3.60e-02	6.34e-03	1060.2575	2276
Axis	6	2.84e-01	7.72e-04	4.01e-02	3.73e-03	999.0325	3930
Kotak	3	3.38e-01	1.89e-03	4.91e-02	1.07e-02	1636.4549	1711
Kotak	6	4.03e-01	1.27e-03	5.15e-02	7.15e-03	1494.8101	2922

Table 15: A posteriori checks of the CNM solutions at $t = 0$ ($M = N = 400$) on the grid $S_j = S_f^N e^{x_j}$: minimum of $U_j - g_j$, $g_j = \max(K - S_j, 0)$; range of the discrete delta $\Delta_j = (U_{j+1} - U_j)/(S_{j+1} - S_j)$; minimum of the discrete gamma Γ_j (second divided difference)

Bank	T (months)	$S_f(T)$	$\min_j(U_j - g_j)$	$\min_j \Delta_j$	$\max_j \Delta_j$	$\min_j \Gamma_j$
SBI	3	670.8644	0.00e+00	-0.9954	-0.0000	2.29e-28
SBI	6	706.8651	0.00e+00	-0.9946	-0.0000	2.10e-18
CBI	3	45.3332	0.00e+00	-0.9981	-0.0000	2.17e-10
CBI	6	48.9055	0.00e+00	-0.9972	-0.0000	3.26e-09
Axis	3	1060.2575	0.00e+00	-0.9950	-0.0000	1.66e-31
Axis	6	999.0325	0.00e+00	-0.9941	-0.0000	2.77e-20
Kotak	3	1636.4549	0.00e+00	-0.9936	-0.0000	1.00e-41
Kotak	6	1494.8101	0.00e+00	-0.9924	-0.0000	7.44e-27

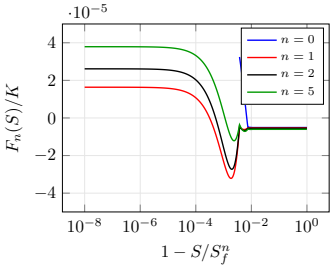
Table 16: Replication study of the two-pass LSM (10^5 paths per pass, 20 independent replications per contract, seeds $10^5 q + 1000i + 10j + 1$ and $10^5 q + 1000i + 10j + 2$, $q = 1, \ldots, 20$). Bias: mean over the replications minus the integral-equation value, averaged over the spot prices (range over the spot prices in brackets); s.e.: mean reported single-run standard error; s.d.: standard deviation over the replications, averaged over the spot prices; last column: number of runs below the reference

data set	mean bias	range of bias	s.e.	s.d.	runs below
SBI, 3 m	-7.10e-02	[-9.29e-02, -4.29e-02]	7.54e-02	8.03e-02	98/120
SBI, 6 m	-1.04e-01	[-1.37e-01, -7.99e-02]	9.72e-02	8.87e-02	103/120
CBI, 3 m	-7.78e-03	[-9.87e-03, -4.79e-03]	1.08e-02	1.18e-02	92/120
CBI, 6 m	-8.08e-03	[-1.14e-02, -4.38e-03]	1.25e-02	1.21e-02	75/100
Axis, 3 m	-1.15e-01	[-1.38e-01, -8.20e-02]	1.12e-01	1.05e-01	104/120
Axis, 6 m	-1.16e-01	[-1.41e-01, -9.65e-02]	1.32e-01	1.39e-01	96/120
Kotak, 3 m	-1.51e-01	[-1.74e-01, -1.28e-01]	1.43e-01	1.40e-01	104/120
Kotak, 6 m	-1.79e-01	[-2.22e-01, -1.12e-01]	1.66e-01	1.63e-01	102/120

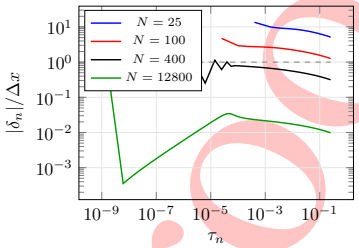
every step F_n had exactly one sign change. F_n is not monotone on the whole interval, however: in 3196 of the 3200 steps it is strictly increasing from twice the distance of the root up to S_f^n, i.e., in a neighbourhood of the root (in the remaining four steps, steps 7-9 for CBI, F_n has a small non-monotone variation in this neighbourhood but still a single sign change), whereas further below the root it is negative but its divided differences change sign (there the trial boundary is so low that the solution near the front is close to the payoff, and $\Phi_n(S)$ follows S closely). The root is therefore unique at the resolution of the scan, and the bracketing, which only uses the sign of F_n, always finds it, whereas secant or Newton steps started far below the root may fail. Figure 2(a) shows F_n at the first steps for the most volatile data set (CBI, three months) as a function of $1 - S/S_f^n$. These findings are restricted to the tested parameter sets; they are numerical evidence, not a proof of existence or uniqueness of the root.

In Figure 3, the plots (a) and (b) further illustrate the relationship between the prices of American and European put options for the State Bank of India (three months). The American put value lies above

Corrected Proof

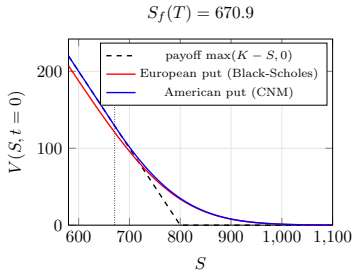


(a) $F_n(S)/K$ for the first steps (CBI, 3 months, CNM, $M = N = 400$).

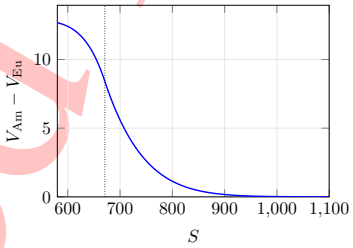


(b) $|\delta_n|/\Delta x$ against τ_n (CBI, 3 months, CNM, graded mesh, $M = 800$).

Figure 2: (a) The function F_n of the boundary equation (26), scaled by K, against the relative distance $1 - S/S_f^n$ at the steps $n = 0, 1, 2, 5$; each has a single zero (values beyond the plotted range are clipped). (b) Shift-to-cell ratios for $N = 25$, 100, 400 and 12800 time steps; the dashed line marks one cell (Section 5.2.1).

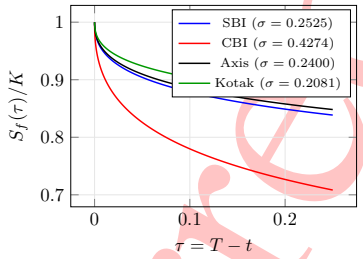


(a) American (CNM) and European put values.

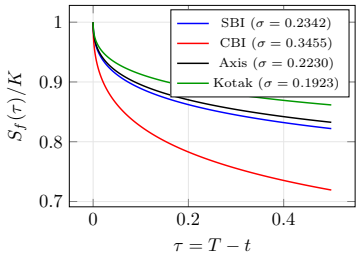


(b) Early exercise premium.

Figure 3: European and American put option prices at $t = 0$ for SBI (three months, $K = 800$, $\sigma = 0.2525$, $r = 0.065$); the dotted line marks $S_f(T)$, the exercise boundary at the valuation date



(a) Three months.

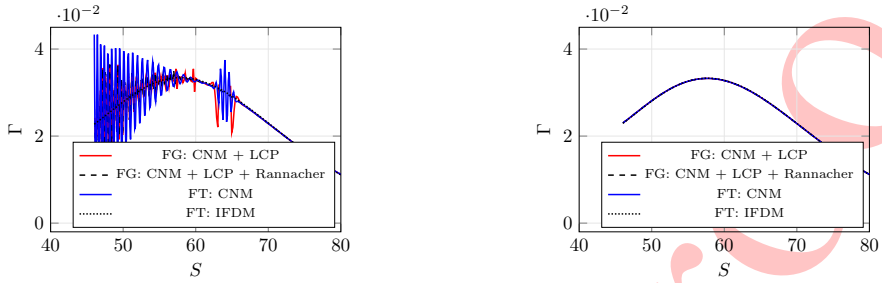


(b) Six months.

Figure 4: Optimal exercise boundaries $S_f(\tau)/K$ as functions of the time to expiry $\tau = T - t$ computed by the CNM ($M = N = 400$)

the European value (Black-Scholes formula) and coincides with the payoff for $S \leq S_f(T) = 670.86$; the early exercise premium $V_{\text{Am}} - V_{\text{Eu}}$ is largest near the exercise boundary and decays as S increases. Similar behaviour is observed for the remaining datasets considered in this paper. The exercise boundaries of all eight data sets are shown in Figure 4 as functions of the time to expiry $\tau = T - t$: they start at $S_f(0) = K$ at expiry with the square-root-logarithmic behaviour discussed in Section 2.1 and decrease with time to expiry , reaching $S_f(T)$ at the valuation date $\tau = T$ ($t = 0$); the lower the volatility, the closer the boundary stays to the strike.

Corrected Proof



(a) $N = 50$. **(b)** $N = 200$.

Figure 5: Discrete gamma $\Gamma = \partial^2 V/\partial S^2$ at $t = 0$ for CBI (three months): fixed-grid (FG) CNM with exact LCP, with and without Rannacher start, and front-tracking (FT) CNM and IFDM. The spike of the FG-CNM at the strike ($S = 64$) is clipped.

Now, to ensure that the simulated results for American put prices are indeed higher than those of European puts, more computations are done and the results are presented in Table 17. The European values are computed from the Black-Scholes formula, so the last column is the early exercise premium. It is positive in all cases and largest for in-the-money options and for the six-month contracts; for CBI (six months, $S_0 = 45 < S_f(T)$) the American put is exercised immediately and its value is the payoff $K - S_0 = 23$.

5.7 Accuracy-matched comparison of run times

Run times are only meaningful together with the accuracy that they buy. Table 18 therefore compares the five methods at matched accuracy. For three data sets (SBI, CBI and Kotak, three months) each method was run on a ladder of discretisation levels: EFDM with $M = 25,\dots,400$ and N from Theorem 3(ii); IFDM with $M = 50,\dots,400$ and $N = M^2/25$; CNM with $M = 50,\dots,1600$ and $N = M$; BBSR with $N_b = 250,\dots,16000$; LSM with 10^4 and 10^5 paths per pass. The error is $e_V = \max_j |V(S_0^{(j)}) - V_{\mathrm{IE}}(S_0^{(j)})|$ over the six spot prices of Table 13 with respect to the integral-equation reference (type (ES3)). For each target $e_V/K \le 10^{-4}, 10^{-5}, 10^{-6}$ the table gives the cheapest level that meets it and the run time for all six prices, measured as specified in Section 5.6. In all cases the finer levels of the ladder also meet the target.

Within the finite difference methods, the CNM with $N = M$ is the cheapest at $10^{-6}K$ for SBI and CBI and at $10^{-5}K$ for CBI; in the other cases (all three data sets at $10^{-4}K$, SBI and Kotak at $10^{-5}K$, Kotak at $10^{-6}K$) the explicit scheme on its coarser levels is faster. The IFDM is limited by its first-order temporal error and does not reach $10^{-6}K$ in the tested range. The LSM does not reach $10^{-4}K$ with 10^5 paths (its errors are 1.6-2.8 $\times\, 10^{-4}K$). For the six spot prices of these tables, the binomial method BBSR is the fastest method at the strictest target $10^{-6}K$ for all three data sets (0.12-0.38 seconds) and at $10^{-5}K$ for CBI and Kotak, whereas at $10^{-4}K$ (and for SBI at $10^{-5}K$) the explicit scheme on its coarsest levels is the fastest (0.01-0.02 seconds, against 0.03-0.05 seconds for BBSR); at these looser targets the run times of both methods are only a few hundredths of a second. Two qualifications apply. First, the cost of BBSR is proportional to the number of spot prices, whereas one finite difference run gives the complete price curve, the exercise boundary $S_f(\tau)$ and the Greeks. Second, the finite difference codes perform a scalar root search with about 7 tridiagonal solves in every time step, and this loop is relatively expensive in an interpreted language, while the BBSR trees are evaluated with vectorised operations. The advantage of

Corrected Proof

Table 17: European (Black-Scholes) and American (CNM, $M = N = 400$) put option values and early exercise premium (American minus European) ($r = 0.065$; K, T, σ as in Table 2)

Bank	S_0	European Put	American Put	Premium
SBI (3 months)	740	66.4787	69.5450	3.0663
	760	53.9759	56.2063	2.2304
	775	45.6607	47.4032	1.7425
	785	40.6258	42.0981	1.4723
	800	33.8244	34.9612	1.1368
	820	26.1029	26.8994	0.79649
SBI (6 months)	805	68.8849	74.2807	5.3958
	820	61.0017	65.4969	4.4952
	835	53.7788	57.5138	3.7350
	855	45.1484	48.0539	2.9054
	870	39.3963	41.7955	2.3992
	885	34.2301	36.2061	1.9760
CBI (3 months)	50	13.8226	14.2628	0.44026
	55	9.9714	10.2231	0.25166
	58	8.0053	8.1830	0.17776
	62	5.8150	5.9253	0.11028
	65	4.4885	4.5648	0.07632
	70	2.8184	2.8590	0.04060
CBI (6 months)	45	21.1656	23.0000	1.8344
	55	12.7941	13.5824	0.78824
	60	9.4615	9.9404	0.47889
	70	4.7223	4.8935	0.17119
	75	3.2058	3.3067	0.10089
	85	1.3860	1.4202	0.03425
Axis (3 months)	1175	89.0582	93.2220	4.1638
	1200	74.2660	77.4358	3.1697
	1220	63.6630	66.1947	2.5317
	1244	52.3741	54.2924	1.9183
	1260	45.6959	47.2828	1.5869
	1285	36.5562	37.7273	1.1711
Axis (6 months)	1130	88.9168	96.2878	7.3710
	1160	73.7642	79.3470	5.5828
	1175	66.9256	71.7727	4.8471
	1205	54.6713	58.3078	3.6364
	1220	49.2268	52.3691	3.1423
	1250	39.6156	41.9511	2.3355
Kotak (3 months)	1800	100.099	105.409	5.3108
	1820	89.0573	93.5275	4.4701
	1840	78.8554	82.6041	3.7486
	1860	69.4860	72.6179	3.1319
	1880	60.9334	63.5402	2.6068
	1900	53.1740	55.3355	2.1615
Kotak (6 months)	1640	111.101	122.636	11.5350
	1680	90.8111	99.3507	8.5396
	1700	81.7161	89.0410	7.3249
	1740	65.5510	70.9071	5.3561
	1760	58.4384	63.0043	4.5659
	1800	46.0207	49.3184	3.2977

Table 18: Accuracy-matched comparison (three months; type (ES3)): for each target e_V/K, the cheapest level of each method that meets it, i.e., M (EFDM, IFDM, CNM), N_b (BBSR) or paths per pass (LSM), and in parentheses the run time in seconds for all six spot prices (median of three runs, MATLAB R2023b, environment of Section 5.6). "–": not reached in the tested range. Couplings: EFDM N from Theorem 3(ii), IFDM $N = M^2/25$, CNM $N = M$, BBSR trees N_b and $N_b/2$

data set	target e_V/K	EFDM	IFDM	CNM	BBSR	LSM
SBI, 3 m	10^{-4}	25 (0.01)	100 (0.11)	100 (0.04)	250 (0.04)	–
SBI, 3 m	10^{-5}	50 (0.02)	400 (2.75)	400 (0.18)	250 (0.04)	–
SBI, 3 m	10^{-6}	400 (0.89)	–	800 (0.49)	1000 (0.31)	–
CBI, 3 m	10^{-4}	25 (0.02)	100 (0.11)	100 (0.04)	250 (0.05)	–
CBI, 3 m	10^{-5}	100 (0.10)	400 (3.12)	200 (0.07)	250 (0.05)	–
CBI, 3 m	10^{-6}	400 (2.75)	–	800 (0.58)	1000 (0.38)	–
Kotak, 3 m	10^{-4}	25 (0.01)	100 (0.10)	100 (0.04)	250 (0.03)	–
Kotak, 3 m	10^{-5}	100 (0.04)	400 (2.84)	400 (0.20)	250 (0.03)	–
Kotak, 3 m	10^{-6}	400 (0.61)	–	1600 (1.48)	500 (0.12)	–

the front-tracking schemes is therefore the accurate exercise boundary and the information obtained in a single run, not the raw speed for a few prices.

Corrected Proof

Table 19: Sensitivity to the free-boundary update procedure (CNM, $M = N = 400$, three months): computed boundary $S_f^N \approx S_f(T)$, its error $e_S = |S_f^N - S_f^{\mathrm{ref}}(T)|$ with respect to the integral-equation reference, maximal price error e_V over the six spot prices with respect to BBSR (both of type (ES3)), and mean number of evaluations of F_n per time step

Bank	update	solver	S_f^N	e_S	e_V	evals/step
SBI	(U1) ghost point, $O(\Delta x^2)$	Brent, $10^{-12}K$	670.8644	3.47e-03	3.89e-03	7.0
		Brent, $10^{-6}K$	670.8644	3.41e-03	3.89e-03	5.8
		single pass	diverges ($S_f^N = 0.4232$)			1.0
	(U2) one-sided, $O(\Delta x^2)$	Brent, $10^{-12}K$	670.8924	3.15e-02	4.33e-03	6.8
		Brent, $10^{-6}K$	670.8924	3.15e-02	4.33e-03	5.6
		single pass	diverges ($S_f^N = 0.2321$)			1.0
	(U3) one-sided, $O(\Delta x)$	Brent, $10^{-12}K$	670.1523	7.09e-01	2.82e-03	7.1
		Brent, $10^{-6}K$	670.1522	7.09e-01	2.82e-03	5.8
		single pass	diverges ($S_f^N = 0.1375$)			1.0
CBI	(U1) ghost point, $O(\Delta x^2)$	Brent, $10^{-12}K$	45.3332	8.61e-04	1.69e-04	6.7
		Brent, $10^{-6}K$	45.3332	8.57e-04	1.69e-04	5.5
		single pass	diverges ($S_f^N = 0.0165$)			1.0
	(U2) one-sided, $O(\Delta x^2)$	Brent, $10^{-12}K$	45.3351	2.75e-03	2.27e-04	7.0
		Brent, $10^{-6}K$	45.3351	2.75e-03	2.27e-04	5.4
		single pass	diverges ($S_f^N = 0.0145$)			1.0
	(U3) one-sided, $O(\Delta x)$	Brent, $10^{-12}K$	45.3328	4.59e-04	1.55e-04	6.7
		Brent, $10^{-6}K$	45.3328	4.54e-04	1.55e-04	5.5
		single pass	diverges ($S_f^N = 0.0092$)			1.0

5.8 Sensitivity to the free-boundary update procedure

In Table 19, we compare the three update equations (24)-(25) combined with three ways of solving the coupled equation (26): Brent's method to a tight ($10^{-12}K$) and to a loose ($10^{-6}K$) tolerance, and a single predictor pass without iteration (the boundary is extrapolated linearly in τ (for $\ln S_f$) from the two previous levels, limited to S_f^n, one step is taken, and the update formula is applied once, the result again being limited to S_f^n). The results lead to three conclusions. (a) Provided the coupled equation is solved, the option values are insensitive to the update rule: the maximal price errors differ by about 1.5×10^{-3} (SBI) and less than 8×10^{-5} (CBI) between (U1)-(U3), and they are dominated by the discretisation error of the scheme. (b) The exercise boundary is more sensitive: the first-order rule (U3) shifts $S_f(T)$ by 0.71 (0.09% of K) for SBI, the one-sided second-order rule (U2) by 0.03, while the ghost-point rule (U1), which uses the curvature condition of Lemma 1, gives the most accurate boundary; for CBI all three rules give $S_f(T)$ to within 3×10^{-3}, the error being dominated there by the temporal discretisation. (c) The solution of (26) must not be skipped: with a single predictor pass the boundary is no longer determined consistently; it collapses towards zero. Relaxing the tolerance of Brent's method from $10^{-12}K$ to $10^{-6}K$ changes $S_f(T)$ by at most 7.9×10^{-5} (i.e., $10^{-7}K$), leaves all price errors unchanged in the digits shown, and saves about 18% of the evaluations; the method is therefore robust with respect to the stopping criterion.

5.9 Deep in-the-money and deep out-of-the-money options

In Table 21, we extend the comparison to $0.5 \le S_0/K \le 1.8$ for SBI (moderate volatility) and CBI (high volatility).

Deep in the money. If $S_0 \le S_f(T)$ ($S_0/K \le 0.8$ for SBI; $S_0/K \le 0.7$ for CBI), immediate exercise is optimal, and the front-tracking θ-scheme for the American put returns the payoff $K - S_0$ exactly; the only

Corrected Proof

Table 20: Truncated endpoint $x_{\max} = 1.5$ (CNM, $M = N = 400$), relative to K: position of the endpoint at the valuation date, exact value $\varepsilon_{\mathrm{tr}} = V(S_f(T)e^{x_{\max}}, T)$ replaced by zero (integral-equation solution), largest discarded interpolated value $|(\Pi_n U^n)_M|$, and maximal changes of the six prices and of $S_f(T)$ when $x_{\max}$ is enlarged to 3 (same Δx, $M = 800$, $N = 400$)

data set	$S_f(T)e^{x_{\max}}/K$	$\varepsilon_{\mathrm{tr}}/K$	$\max_n \lvert(\Pi_n U^n)_M\rvert/K$	$\max \lvert\Delta V\rvert/K$	$\lvert\Delta S_f(T)\rvert/K$
SBI, 3 m	3.758	2.8e-28	1.7e-29	0	0
SBI, 6 m	3.684	1.3e-17	3.3e-19	0	0
CBI, 3 m	3.175	1.4e-09	3.9e-11	0	0
CBI, 6 m	3.223	3.5e-08	6.7e-10	3.3e-18	0
Axis, 3 m	3.801	2.0e-31	1.5e-32	0	0
Axis, 6 m	3.731	2.0e-19	5.2e-21	0	0
Kotak, 3 m	3.912	2.8e-42	6.3e-43	0	0
Kotak, 6 m	3.861	3.3e-26	1.1e-27	0	0

requirement is an accurate exercise boundary. In this region the European value is considerably smaller than the American value (e.g., 387.1 versus 400 for SBI at $S_0 = 0.5K$), which illustrates the importance of the early exercise feature. Between $S_f(T)$ and K the absolute errors are of the order $10^{-4}K$ or smaller.

Deep out of the money. For $S_0 > K$, the absolute errors decrease rapidly with S_0 (to about 4×10^{-7} at $S_0 = 1.8K$), but the option values decrease even faster, so the relative error grows, to about 1.6% for SBI at $S_0 = 1.8K$, where the option value is 2.2×10^{-5} (i.e., $3 \times 10^{-8}K$). At this level the accuracy of the reference itself is a limiting factor, and such values are irrelevant in practice. The truncation of the domain plays no role: with $x_{\max} = 1.5$ the grid extends to $S \approx 4.48\,S_f(\tau)$, i.e., beyond $3.7K$ for SBI and $3.1K$ for CBI, and enlarging it to $x_{\max} = 2.5$ (with the same Δx) changes the values by less than 10^{-6}. For options still further out of the money, or for longer maturities and higher volatilities, $x_{\max}$ should be chosen such that $S_f(T)e^{x_{\max}}$ exceeds S_0 by several standard deviations, e.g., $x_{\max} \geq \ln(S_0/S_f(T)) + 5\sigma\sqrt{T}$.

Effect of the truncated endpoint. Table 20 quantifies the two differences at $x = x_{\max}$ that were distinguished in Section 3.1, for all eight data sets and the CNM with $M = N = 400$. The exact value replaced by the truncation condition, $\varepsilon_{\mathrm{tr}}$ in (12), is computed from the integral-equation representation (38). It is largest for the most volatile six-month data (CBI, $3.5 \times 10^{-8}K$) and below $10^{-16}K$ for the six data sets with $\sigma \leq 0.26$. By (13) the truncation therefore changes the option values by at most $3.5 \times 10^{-8}K$ (2.4×10^{-6} for CBI, six months). This is more than an order of magnitude below the smallest discretisation error for that data set in Table 14 (5.2×10^{-5}, EFDM), and for all other data sets the bound is smaller by many further orders of magnitude. The interpolated values at x_M that are discarded are smaller still (at most $6.7 \times 10^{-10}K$). Finally, enlarging the domain to $x_{\max} = 3$ with the same Δx ($M = 800$) leaves all eight boundaries $S_f(T)$ and 47 of the 48 prices of Table 13 unchanged to all digits in double precision; one price (CBI, six months) changes by 2×10^{-16}, one unit in the last place: the influence of the endpoint decays rapidly with the distance from $x_{\max}$, and at S_0 and at the front it lies below the rounding level. Hence the truncation does not affect the reported results.

5.10 Non-smoothness of the payoff at the strike

The payoff $\max(K - S, 0)$ has a kink at $S = K$, and this is a well-known source of difficulties for finite difference methods, in particular for the Crank-Nicolson scheme, which is A-stable but not L-stable and hence damps high-frequency errors only weakly [24]. The present method handles it as follows.

Corrected Proof

Table 21: Dependence on moneyness (three months, CNM with $N = 400$, graded mesh): reference (BBSR, $N_b = 20000$), European value, CNM value with $x_{\max} = 1.5$ ($M = 400$), and absolute ($|V - V_{\mathrm{BBSR}}|$) and relative ($|V - V_{\mathrm{BBSR}}|/V_{\mathrm{BBSR}}$) errors for $x_{\max} = 1.5$ and $x_{\max} = 2.5$ ($M = 667$, essentially the same Δx) (type (ES3))

					$x_{\max} = 1.5$		$x_{\max} = 2.5$	
Bank	S_0/K	BBSR	European	CNM	abs. err.	rel. err.	abs. err.	rel. err.
SBI	0.5	400.000	387.105	400.000	0.0e+00	0.0e+00	0.0e+00	0.0e+00
	0.7	240.000	227.195	240.000	0.0e+00	0.0e+00	0.0e+00	0.0e+00
	0.8	160.000	149.002	160.000	0.0e+00	0.0e+00	0.0e+00	0.0e+00
	0.9	84.7024	80.5359	84.7005	1.9e-03	2.2e-05	1.9e-03	2.2e-05
	1.0	34.9651	33.8244	34.9612	3.9e-03	1.1e-04	3.9e-03	1.1e-04
	1.1	11.1164	10.8594	11.1140	2.4e-03	2.2e-04	2.4e-03	2.2e-04
	1.2	2.7627	2.7146	2.7622	5.2e-04	1.9e-04	5.2e-04	1.9e-04
	1.4	0.09300	0.09194	0.09312	1.1e-04	1.2e-03	1.1e-04	1.2e-03
	1.6	0.00174	0.00173	0.00175	1.1e-05	6.1e-03	1.1e-05	6.1e-03
	1.8	0.00002	0.00002	0.00002	3.7e-07	1.6e-02	3.7e-07	1.6e-02
CBI	0.5	32.0000	30.9704	32.0000	0.0e+00	0.0e+00	0.0e+00	0.0e+00
	0.7	19.2000	18.4355	19.2000	0.0e+00	0.0e+00	0.0e+00	0.0e+00
	0.8	13.2242	12.8383	13.2242	6.1e-05	4.6e-06	6.1e-05	4.6e-06
	0.9	8.4379	8.2515	8.4378	1.4e-04	1.6e-05	1.4e-04	1.6e-05
	1.0	4.9883	4.9018	4.9881	1.7e-04	3.4e-05	1.7e-04	3.4e-05
	1.1	2.7495	2.7108	2.7493	1.4e-04	5.2e-05	1.4e-04	5.2e-05
	1.2	1.4261	1.4093	1.4260	8.9e-05	6.2e-05	8.9e-05	6.2e-05
	1.4	0.33234	0.32942	0.33233	4.8e-06	1.4e-05	4.8e-06	1.4e-05
	1.6	0.06767	0.06720	0.06768	1.3e-05	1.9e-04	1.3e-05	1.9e-04
	1.8	0.01268	0.01260	0.01269	8.0e-06	6.3e-04	8.0e-06	6.3e-04

(i) At $\tau = 0$ the free boundary starts at $S_f(0) = K$, i.e., exactly at the kink, and in the variable $x = \ln(S/S_f)$ the initial function is $u(x,0) = 0$ for $x > 0$, which is smooth. The kink is thus removed from the computational domain.

(ii) The singularity is not removed but transferred to the free boundary: $S_f(\tau) \sim K(1 - \sigma\sqrt{\tau|\ln\tau|})$, so $s(\tau)$ is unbounded as $\tau \to 0^+$. This singularity is resolved by the graded mesh (14). Table 8 shows the effect: with uniform time steps the CNM option values converge only at a rate of about one, with the graded mesh the rate is two (down to the accuracy floor discussed in Section 5.2).

(iii) Because the grid moves with the boundary, the payoff region never enters the continuation region except through the swept layer $S_f^{n+1} \le S < S_f^n$, where the transfer (16) assigns the exact payoff. No oscillations are generated.

(iv) The option values are hardly affected by the remaining non-smoothness (see tables 8 and 10); its effect is most visible in the Greeks. Table 22 indicates the maximal deviation of the discrete gamma $\Gamma = V_{SS}$ at $t = 0$ on $46 \le S \le 90$ from a smooth reference, and Figure 5 shows Γ for $N = 50$ and $N = 200$ time steps. On a fixed grid, the CNM with only $N = 50$ steps produces an $O(1)$ spurious spike of Γ at the strike, where the payoff has its kink. The Rannacher start (four implicit half steps) removes this spike.

(v) In the front-tracking CNM there is no spike at the strike, because the kink is not in the computational domain; the maximal deviation for $N = 50$ is about 75 times smaller than for the fixed-grid CNM. With very large time steps ($\Delta\tau\sigma^2/\Delta x^2 \approx 500$ for $N = 50$), however, both Crank-Nicolson versions show oscillations of Γ near the exercise boundary, where Γ jumps from 0 to $2rK/(\sigma^2 S_f^2) \approx 0.022$. In the front-tracking scheme such a jump is re-created at every step (through

Corrected Proof

Table 22: Maximal deviation $\max_j |\Gamma_j - \Gamma_{\text{ref}}(S_j)|$ of the discrete gamma at $t = 0$ over the grid nodes with $46 \le S_j \le 90$ from the reference (front-tracking CNM, $M = 800$, $N = 6400$, linearly interpolated); CBI, three months. Fixed grid: $M = 1600$, $S_{\max} = 4K$, uniform time steps, exact LCP; front tracking: $M = 800$, graded mesh

formulation	scheme	$N = 50$	$N = 100$	$N = 200$	$N = 400$
fixed grid	CNM + LCP	1.51e+00	1.21e-01	5.65e-05	2.69e-05
	CNM + LCP + Rannacher	1.12e-02	1.31e-03	5.76e-05	2.59e-05
	IFDM + LCP	2.31e-04	1.17e-04	6.01e-05	3.72e-05
front tracking	CNM	2.03e-02	6.12e-04	4.76e-05	9.48e-08
	CNM + Rannacher	2.03e-02	6.12e-04	4.75e-05	9.25e-08
	IFDM	2.88e-04	1.45e-04	7.26e-05	3.63e-05

the swept layer), so the Rannacher start, which only damps the initial data, does not help; these oscillations decay rapidly as N increases and are absent for $N \ge 200$. For the $N = 400$ steps used in Tables 13-15, the front-tracking gamma agrees with the reference to within 10^{-7}.

(vi) The fully implicit scheme is L-stable and never oscillates, but it is only first-order accurate in time.

In summary, the front-tracking formulation removes the strike singularity from the computational domain, the graded mesh resolves the singular behaviour of the free boundary near expiry, and a moderate number of time steps (here $N \ge 200$) avoids Crank-Nicolson oscillations of the Greeks near the boundary; and for fixed-grid Crank-Nicolson scheme, a Rannacher start is necessary.

6 Concluding remarks and scope for further research

In this paper, we constructed and analyzed three finite difference methods for solving the Black-Scholes partial differential equation associated with American options on a single asset. The free boundary problem was written in the logarithmic front-tracking variable $x = \ln(S/S_f(\tau))$, in which the boundary velocity S_f'/S_f and the update equation for the exercise boundary appear explicitly; the velocity term was integrated along characteristics on a grid that moves with the boundary, and the boundary was updated by a ghost-point formula based on the curvature condition $\frac{1}{2}\sigma^2 S_f^2 V_{SS}(S_f^+) = rK$, the resulting scalar equation being solved at every time level by a safeguarded root finder. The boundary condition at $S = 0$ was corrected to $V(0,t) = K$. While the primary emphasis was on the formulation and implementation of the Crank-Nicolson method, the forward difference in time and central difference in space (FTCS) and backward difference in time and central difference in space (BTCS) schemes were considered for comparison purposes. Because the difference operator has constant coefficients in the variable x, the stability of their linear steps for a prescribed boundary position could be analysed exactly: we proved unconditional ℓ_2-stability of the implicit and Crank-Nicolson diffusion steps, the sharp time-step bound $\Delta\tau(2\sigma^2/\Delta x^2 + r) \le 2$ for the explicit step, and a discrete maximum principle (unconditionally for the implicit step, under time-step restrictions for the other two). A single step of the interpolation along characteristics was shown analytically to be von Neumann stable, and its one-step error was bounded with constants that do not depend on the size of the shift, which in the first steps of coarse time meshes spans many cells, or on the mesh size. We also pointed out what this analysis does not cover (the nonlinear coupling through the free boundary : there is no existence or uniqueness result for the boundary equation and no stability or convergence theorem for the fully coupled scheme) and complemented it by a convergence study against independent reference solutions , in particular an integral-equation solution for the exercise boundary and the option values, by numerical checks of existence and uniqueness of the

Corrected Proof

root of the boundary equation, and by a posteriori checks of the discrete complementarity conditions. In these experiments the errors of all three schemes with respect to the independent references decreased under refinement, with observed orders close to two in space, and the Crank-Nicolson prices showed second-order temporal error reduction (grid-difference evidence) on the graded mesh down to errors of about 10^{-5} at $M = 800$, below which the errors depend irregularly on the number of time steps. These are numerical observations for the tested parameter sets, not consequences of a theorem.

The status of the results can be summarised as follows.

(i) *Proved* (Section 4), for a prescribed boundary position S_f^{n+1} and statements about single linear steps: local consistency, of order one (EFDM, IFDM) or two (CNM) in time and two in space, away from the corner $(x,\tau) = (0,0)$; von Neumann and ℓ_2-stability of the diffusion step; the discrete maximum principle (unconditionally for the IFDM, under time-step restrictions for the EFDM and CNM); von Neumann stability of a single transfer step along characteristics and a one-step interpolation bound with constants independent of the size of the shift and the mesh size. For the continuous problem, the error of the domain truncation is bounded by (13).

(ii) *Not proved:* existence and uniqueness of the root of the boundary equation (26), and stability and convergence of the fully coupled nonlinear scheme.

(iii) *Observed numerically*, for the parameter sets of this paper: decrease of the errors with respect to the integral-equation reference with the orders reported in Table 7 (type (ES3)), temporal error reduction against same-grid references in Table 8 (type (ES2)); a single sign change of F_n at the resolution of the scan and no failure of the root search (Section 5.6.1); and the discrete complementarity conditions (Table 15).

The evidence in (iii) supports, but does not replace, a convergence proof for the coupled scheme.

Among the three finite difference schemes, the explicit scheme was in most cases the cheapest at the two looser accuracy targets and the Crank-Nicolson method with $N = M$ at the strictest target for two of the three data sets tested (Table 18); at $M = N = 400$ its errors were below $6 \times 10^{-6}K$, with the complete price curve and the exercise boundary obtained in less than one second in the computing environment specified in Section 5.6. For the six spot prices per contract, the binomial method with Richardson extrapolation was the fastest method at the strictest accuracy target, and comparable in speed to the explicit scheme at the looser targets (Table 18); the advantage of the front-tracking schemes lies in the accurate exercise boundary and the complete solution obtained in one run, not in the speed for a few prices. The obtained option values were found to be comparable with those generated using the stochastic framework of [19], whose errors are, however, one to two orders of magnitude larger. Additional results were presented using the Crank-Nicolson method to verify that American put option prices remain higher than the corresponding European put option prices. It is important to note that the early exercise constraint must be handled consistently: in the fixed-grid formulation, applying the projection $V \leftarrow \max(V, K - S)$ after an implicit or Crank-Nicolson step is an $O(\Delta\tau)$ splitting of the discrete complementarity problem and reduces the Crank-Nicolson scheme to first order in time, whereas with the exact solution of the discrete LCP (Brennan-Schwartz algorithm) the temporal errors are 8 to 16 times smaller and decay faster.

The volatilities used are historical close-to-close volatilities; range-based estimators give 4-9% lower values for the Central Bank of India data and change the American put value by less than 5%. The

Corrected Proof

risk-free rate is the policy repo rate of the Reserve Bank of India (6.50%). Dividends were omitted; a continuous dividend yield of 1% (2%) raises the three-month put values by 0.8-2.0% (1.6-4.1%) and lowers the exercise boundary accordingly. Since Indian single-stock options are European-style, the application is a model-parameter study of hypothetical American contracts and not an empirical validation against traded American options. Once the coupled boundary equation is solved, the option values are insensitive to the particular boundary-update formula, whereas a non-iterated update does not determine the boundary consistently: the computed boundary collapses towards zero (Table 19). The method treats deep in-the-money options exactly (immediate exercise) and deep out-of-the-money options accurately in absolute terms, provided the computational domain is large enough (for the data sets considered, the truncated endpoint changes the option values by at most $3.5 \times 10^{-8}K$, and in the computations by less than the rounding error); and the non-smoothness of the payoff at the strike is removed from the computational domain by the transformation and transferred to the free boundary near expiry, where it is resolved by the graded time mesh; with very large time steps the Crank-Nicolson scheme still produces oscillations of the gamma near the exercise boundary, which disappear for moderate numbers of time steps. Due to space limitations, numerical experiments were restricted to three- and six-month datasets; however, the estimated volatilities for 12-month data were 0.2972, 0.4945, 0.2457, and 0.2366 for State Bank of India, Central Bank of India, Axis Bank, and Kotak Mahindra Bank, respectively.

As a direction for future research, we are investigating the extension of the proposed methodologies to American put option pricing problems involving multiple dividend payments. In this paper, we consider the non-dividend-paying case (and, for comparison, a continuous dividend yield); therefore, our initial objective is to generalize the framework to incorporate a single dividend payment, followed by its extension to problems with multiple dividends. A proof of convergence of the fully coupled front-tracking scheme also remains open. Furthermore, we recognize the potential challenges associated with the application of the Crank-Nicolson approach for the accurate computation of option Greeks. These issues will be investigated concurrently while extending the proposed methodology to both single- and multiple-dividend American option pricing problems.

Acknowledgements.

The first author acknowledges the financial support provided by Sagar University through the University Grants Commission (UGC), India, in the form of a Non-NET Scholarship for PhD research at Central Universities of India. The authors also wish to thank the two reviewers for their constructive comments, which led to a substantial improvement of the paper.

Supplementary material.

Supplementary file S1: `Three_and_six_month_data_files.xlsx`, the unadjusted daily NSE prices of the eight bank-maturity windows used in Section 5 (one sheet per window).

Competing interests:

The authors declare that they have no competing interests.

Corrected Proof

Declaration of generative AI and AI-assisted technologies in the writing process.

During the preparation of this work, the authors have used Claude to improve the readability and language of the manuscript. After using these tools, the authors reviewed and edited the content as needed and take full responsibility for the content of the publication.

References

[1] G. Barles, J. Burdeau, M. Romano, N. Samsoen, *Critical stock price near expiration*, Math. Finance **5(2)** (1995) 77-95.

[2] M.J. Brennan, E.S. Schwartz, *The valuation of American put options*, J. Finance **32(2)** (1977) 449-462.

[3] R.P. Brent, *Algorithms for Minimization without Derivatives*, Prentice-Hall, Englewood Cliffs, NJ, 1973.

[4] M. Broadie, J. Detemple, *American option valuation: new bounds, approximations, and a comparison of existing methods*, Rev. Financ. Stud. **9(4)** (1996) 1211-1250.

[5] R. Company, V.N. Egorova, L. Jódar, *Solving American option pricing models by the front fixing method: numerical analysis and computing*, Abstr. Appl. Anal. **2014** (2014) 146745.

[6] P. Carr, R. Jarrow, R. Myneni, *Alternative characterizations of American put options*, Math. Finance **2(2)** (1992) 87-106.

[7] J.C. Cox, S.A. Ross, M. Rubinstein, *Option pricing: A simplified approach*, J. Financ. Econ. **7(3)** (1979) 229-263.

[8] M. Falcone, R. Ferretti, *Semi-Lagrangian Approximation Schemes for Linear and Hamilton-Jacobi Equations*, SIAM, Philadelphia, 2014.

[9] S. Fallah, F. Mehrdoust, *A study of American options under stochastic volatility and double exponential jumps*, J. Math. Model. **13(2)** (2025) 467-484.

[10] R. Fazio, A. Insana, A. Jannelli, *A front-fixing implicit finite difference method for the American put options model*, Math. Comput. Appl. **26(2)** (2021) 30.

[11] P.A. Forsyth, K.R. Vetzal, *Quadratic convergence for valuing American options using a penalty method*, SIAM J. Sci. Comput. **23(6)** (2002) 2095-2122.

[12] M.B. Garman, M.J. Klass, *On the estimation of security price volatilities from historical data*, J. Business **53(1)** (1980) 67-78.

[13] F. Gatta, V. Schiano Di Cola, F. Giampaolo, F. Piccialli, S. Cuomo, *Meshless methods for American option pricing through Physics-Informed Neural Networks*, Eng. Anal. Bound. Elem. **151** (2023) 68-82.

Corrected Proof

[14] S. Ikonen, J. Toivanen, *Operator splitting methods for American option pricing*, Appl. Math. Lett. **17(7)** (2004) 809-814.

[15] S. Ikonen, J. Toivanen, *Operator splitting methods for pricing American options under stochastic volatility*, Numer. Math. **113** (2009) 299-324.

[16] P. Jaillet, D. Lamberton, B. Lapeyre, *Variational inequalities and the pricing of American options*, Acta Appl. Math. **21(3)** (1990) 263-289.

[17] I.J. Kim, *The analytic valuation of American options*, Rev. Financ. Stud. **3(4)** (1990) 547-572.

[18] P.D. Lax, R.D. Richtmyer, *Survey of the stability of linear finite difference equations*, Commun. Pure Appl. Math. **9(2)** (1956) 267-293.

[19] F.A. Longstaff, E.S. Schwartz, *Valuing American options by simulation: A simple least-squares approach*, Rev. Financ. Stud. **14(1)** (2001) 113-147.

[20] M. Maidoumi, M. Zahid, B. Daafi, *Pricing American option under exponential Lévy jump-diffusion model using random forest instead of least square regression*, J. Math. Model. **11(2)** (2023) 229-244.

[21] B.F. Nielsen, O. Skavhaug, A. Tveito, *Penalty and front-fixing methods for the numerical solution of American option problems*, J. Comput. Finance **5(4)** (2002) 69-97.

[22] S.M. Nuugulu, K.C. Patidar, D.T. Tarla, *A physics-informed neural network approach for solving time fractional Black-Scholes partial differential equations*, Optim. Eng. **26(4)** (2025) 2419-2448.

[23] M. Parkinson, *The extreme value method for estimating the variance of the rate of return*, J. Business **53(1)** (1980) 61-65.

[24] D.M. Pooley, K.R. Vetzal, P.A. Forsyth, *Convergence remedies for non-smooth payoffs in option pricing*, J. Comput. Finance **6(4)** (2003) 25-40.

[25] Reserve Bank of India, *Monetary Policy Statement, 2024-25: Resolution of the Monetary Policy Committee (MPC), December 4-6, 2024*, Press Release 2024-2025/1646, Mumbai, 6 December 2024.

[26] L.C.G. Rogers, S.E. Satchell, *Estimating variance from high, low and closing prices*, Ann. Appl. Probab. **1(4)** (1991) 504-512.

[27] D. Ševčovič, *Analysis of the free boundary for the pricing of an American call option*, European J. Appl. Math. **12(1)** (2001) 25-37.

[28] L. Wu, Y.-K. Kwok, *A front-fixing finite difference method for the valuation of American options*, J. Financ. Eng. **6** (1997) 83-97.

[29] D. Yang, Q. Zhang, *Drift-independent volatility estimation based on high, low, open, and close prices*, J. Business **73(3)** (2000) 477-491.

Corrected Proof